

THE ISOTROPIC DIFFUSION SOURCE APPROXIMATION FOR SUPERNOVA NEUTRINO TRANSPORT

M. LIEBENDÖRFER, S. C. WHITEHOUSE, T. FISCHER

Department of Physics, University of Basel, Klingelbergstr. 82, CH-4056 Basel, Switzerland

Draft version January 21, 2009

ABSTRACT

Astrophysical observations originate from matter that interacts with radiation or transported particles. We develop a pragmatic approximation in order to enable multi-dimensional simulations with basic spectral radiative transfer when the available computational resources are not sufficient to solve the complete Boltzmann transport equation. The distribution function of the transported particles is decomposed into a trapped particle component and a streaming particle component. Their separate evolution equations are coupled by a source term that converts trapped particles into streaming particles. We determine this source term by requiring the correct diffusion limit for the evolution of the trapped particle component. For a smooth transition to the free streaming regime, this 'diffusion source' is limited by the matter emissivity. The resulting streaming particle emission rates are integrated over space to obtain the streaming particle flux. Finally, a geometric estimate of the flux factor is used to convert the particle flux to the streaming particle density, which enters the evaluation of streaming particle-matter interactions. The efficiency of the scheme results from the freedom to use different approximations for each particle component. In supernovae, for example, reactions with trapped particles on fast time scales establish equilibria that reduce the number of primitive variables required to evolve the trapped particle component. On the other hand, a stationary-state approximation considerably facilitates the treatment of the streaming particle component. Different approximations may apply in applications to stellar atmospheres, star formation, or cosmological radiative transfer. We compare the isotropic diffusion source approximation with Boltzmann neutrino transport of electron flavour neutrinos in spherically symmetric supernova models and find good agreement. An extension of the scheme to the multi-dimensional case is also discussed.

Subject headings: supernovae: general—neutrinos—radiative transfer—hydrodynamics—methods: numerical

1. INTRODUCTION

Most applications in computational astrophysics involve matter that is in thermal or reactive equilibrium. Astrophysical observations, however, require information to propagate from the astrophysical site to a terrestrial observer. Hence, the observationally interesting events involve additional particle species that are not trapped in the fluid and must therefore be treated by radiative transfer. In many traditional numerical models, the equilibrated matter is treated in the hydrodynamic limit, while transported particle species are treated by a suitable algorithm of radiative transfer. If this splitting in the numerical method is based on the particle species, it can become extremely challenging and inefficient if the range of conditions in the astrophysical scenario is large. In situations where radiative particles are in thermal or reactive equilibrium, the non-local algorithm of radiative transfer has to be perfectly consistent with the hydrodynamics scheme and capable of handling very stiff source terms in order to evolve the applicable equilibria.

For example core collapse supernova events have challenged computer models for several decades (Colgate & White 1966; Arnett 1966; Bowers & Wilson 1982; Bethe & Wilson 1985; Bruenn 1985; Myra & Bludman 1989). These stellar explosions occur at the end of the life of a massive star when the growing iron core, as the end product of nuclear fusion, becomes unstable against gravitational collapse. The collapse is halted only after nuclear density is reached at the centre. The repulsive strong interaction and the

neutron degeneracy pressure reduce the compressibility of matter so that a sound wave travels outward through the causally connected inner core. It turns into a shock wave when it reaches supersonically accreting matter from the outer layers and, due to dissociation and neutrino losses, stalls within few milliseconds to an initially hydrostatic accretion front, which is thought to slowly expand over several hundreds of milliseconds before the explosion sets in. The new-born protoneutron star (PNS) at the centre of the event has a larger density by many orders of magnitude than the shock-heated and dissociated matter that continues to accumulate behind the accretion front. This accreted matter is subject to a variety of fluid instabilities and asymmetric flow patterns that couple to the energetic neutrino radiation field produced within or close to the surface of the PNS. The emergence of an explosion and the detailed interaction between the multi-dimensional flow and the neutrino field is subject to a long-standing and ongoing debate. See for example (Bethe 1990) for a theoretical description of the scenario or (Bruenn et al. 2006; Dessart et al. 2007; Marek & Janka 2007) for recent axisymmetric computer simulations with spectral neutrino transport.

Several aspects of the core collapse supernova scenario make computer models difficult to perform: The relevant densities in the computational domain range over ten decades from about 10^{15} g/cm³ at the centre of the PNS down to about 10^5 g/cm³ in the outermost layers (the star is much larger but does not dynamically

react to the changes at the centre during the first few hundred milliseconds after bounce). This density range implies very disparate dynamical time scales. At high densities, the weak interaction rates are much faster than the dynamical time scale, while at low density, they are even slower than the evolution time scale. This requires implicit finite differencing of many processes to perform simulations in a reasonable amount of time. Moreover, the gravitational and stored internal energy scales are of order 10^{53} erg, while typical kinetic explosion energies are two orders of magnitude smaller. The presence of a strong shock with near-relativistic infall velocities further challenges the resolution and stability of numerical models. In this very dynamical environment with multi-dimensional fluid instabilities and differential rotation, a computer model has to quantify the exchange of energy between matter and the emitted neutrino field in order to allow statements about the explosion dynamics to be made. As the neutrino cross sections at given matter conditions scale with the square of the neutrino energy, the neutrino transport problem must be considered as a superposition of several single-energy (monochromatic) transport problems, where the geometry of the scattering sphere depends on the neutrino energy and type. This leads to multi-group transport schemes where all propagation quantities are solved in separate energy groups (Mazurek 1975; Arnett 1977). Moreover, stationary-state studies with spherically symmetric Boltzmann neutrino transport showed that the angular distribution of the neutrino propagation directions have also to be taken into account to obtain accurate neutrino heating and cooling rates (Wilson 1971; Mezzacappa & Bruenn 1993; Messer et al. 1998; Yamada et al. 1999; Burrows et al. 2000).

In the mean time, the spherically symmetric Boltzmann transport equation is routinely solved for all neutrino flavours in dynamical models of stellar core collapse and postbounce evolution (Liebendörfer et al. 2001; Rampp & Janka 2002; Thompson et al. 2003; Sumiyoshi et al. 2005). These comprehensive and sophisticated codes treat disparate time scales by implicit finite differencing and require large computational resources. However, due to the enormous density range in the scenario, a considerable fraction of the computational domain is either neutrino-opaque or neutrino-transparent. In a fully neutrino-opaque regime, a numerical solution to the Boltzmann transport equation is rarely more accurate than the solution of the simpler diffusion equation that describes the correct physical limit. Similarly, the angular distribution of the neutrino propagation directions in the far-field free streaming regime is precisely determined by the geometry and emissivity of the distant sources, while an angular discretisation of the Boltzmann equation may lead to discretisation errors. Hence, we suggest that a combination of different approaches to radiative transfer is applied in the same astrophysical simulation. This leads to the concept of an ‘adaptive algorithm’, which should not be regarded as an inconsistency or drawback. On the contrary, it saves computation power that can be invested for better resolution, more input physics, or the coverage of a larger parameter space. Current state-of-the-art supernova models with spectral neutrino transport are performed under the assumption of axisymmetry. As a 2D solution of

the Boltzmann equation is computationally inefficient for the reasons discussed above, different groups either apply 1D Boltzmann solutions in separate angular segments in combination with 2D neutrino advection in opaque regimes (ray-by-ray) (Marek & Janka 2007), resort to the multi-group flux-limited diffusion (MGFLD) approximation (Walder et al. 2005; Ott et al. 2008), or use a combination of both (Bruenn et al. 2006).

Three-dimensional supernova models were hitherto only affordable with ‘grey’ neutrino transport (Fryer & Warren 2004) or with other simple ad hoc approximations to the neutrino physics (Scheck et al. 2004; Ott et al. 2007; Scheidegger et al. 2008). But many features of the supernova should be studied in three spatial dimensions, for example the pattern of the accretion flow (Herant et al. 1994), the standing accretion shock instability (Blondin et al. 2003), the excitation of PNS g-modes (Burrows et al. 2006), and the evolution of magnetic fields (see e.g. Kotake et al. (2006) and references therein). In order to enable three-dimensional supernova models with spectral neutrino transport and in order to accelerate parameter studies with simulations of lower dimensionality, we construct the isotropic diffusion source approximation based on several ideas scattered across the literature. Our algorithm is not meant to compete in accuracy with more detailed solutions of the transport equation in the semi-transparent regime. As the transition from the opaque to the transparent regime will be handled by interpolation and basic geometric considerations, it is important that the approach is verified by an accurate transport solution for every new field of application. Our approach shares this limitation with the well-known flux-limited diffusion approximation. The main advantage of the isotropic diffusion source approximation over the latter is that the fluxes and flux factors in the transparent regime are determined by the non-local distribution of sources rather than the local intensity gradient, which may give an incorrect flux direction. Moreover, the new approach tries to limit the computationally expensive solution of the multi-dimensional diffusion equation to the opaque regime where the diffusion approximation is adequate. The goal is to create a flexible algorithm that efficiently implements only the dominant features of radiative transfer in one consistent framework.

The most obvious method of avoiding the inefficient global application of algorithms is a decomposition of the problem in space, so that one algorithm is used in one subdomain while another algorithm is used in another subdomain (Chick & Cassen 1997). Another approach is the decomposition in the momentum phase space into particles with thermal velocities and particles with supra-thermal velocities. If one treats the thermal particles by an efficient fluid model, a hybrid kinetic/fluid model is obtained (Crouseilles et al. 2004). The isotropic diffusion source approximation described in this article is more similar to the so-called δf -method (Parker & Lee 1993; Brunner et al. 1999). We also decompose the distribution function of the transported particles into a thermal component and a perturbation that is allowed to overlap the thermal part in the entire computational domain and particle phase space. However, in our case, the perturbation is not considered to be small. Inspired by flux-limited diffusion (Levermore & Pomraning 1981),

the evolution of the radiation component is guided by the diffusion limit at large opacities and by the free streaming limit at low opacities. In contrast to flux-limited diffusion, we build our scheme conceptually on approximations of the collision integral rather than particle fluxes. We assume that the free streaming particle flux is dominated by the flux emerging from the diffusive domain so that the sources for the far field can easily be integrated. In the stationary-state limit, the determination of the particle fluxes reduces to the solution of a Poisson equation (Gnedin & Abel 2001). Since the matter interacts according to the local particle abundances and not fluxes, we have to convert the particle fluxes to local particle densities. This is achieved by a geometric estimate of the flux factor as suggested and evaluated by Bruenn in (Liebendörfer et al. 2004).

In Sect. 2 we describe in detail how these concepts enter the framework of the isotropic diffusion source approximation, which we design for the transport of massless fermions through a compressible gas. Its connection to the well-known diffusion limit is made in Appendix A. In Sect. 3, we evaluate the performance of this approximation in comparison with Boltzmann neutrino transport in spherical symmetry. Finally, in Sect. 4, we discuss the extension to multi-dimensional simulations. Details of the finite differencing and implementation are given in Appendix B.

2. THE ISOTROPIC DIFFUSION SOURCE APPROXIMATION (IDSA)

In the IDSA, the separation into hydrodynamics and radiative transfer is not based on particle species, but on the local opacity. One particle species is allowed to have a component that evolves in the hydrodynamic limit, while another component of the same particle species is treated by radiative transfer. The restriction of a chosen radiative transfer algorithm to the more transparent regimes enables the use of more efficient techniques that would not be stable in the full domain. In opaque regimes, on the other hand, one can take advantage of equilibrium conditions to reduce the number of primitive variables that need to be evolved. This algorithmic flexibility can drastically decrease the overall computational cost with respect to a traditional approach.

In the IDSA, we decompose the distribution function of one particle species, f , into an isotropic distribution function of trapped particles, f^t , and a distribution function of streaming particles, f^s . In terms of a linear operator $D()$ describing particle propagation, the transport equation is written as $D(f = f^t + f^s) = C$, where $C = C^t + C^s$ is a suitable decomposition of the collision integral according to the coupling to the trapped (C^t) or streaming (C^s) particle components. The ansatz

$$D(f^t) = C^t - \Sigma \quad (1)$$

$$D(f^s) = C^s + \Sigma, \quad (2)$$

requires that we specify an additional source term Σ , which converts trapped particles into streaming particles and vice versa. We determine it approximately from the requirement that the temporal change of f^t in Eq. (1) has to reproduce the diffusion limit in the limit of small mean free paths. Hence, we call Σ the 'diffusion source'. In regions of large mean free paths, we limit the diffusion source by the local particle emissivity. Once Σ

is determined by the solution of Eq. (1) for the trapped particle component, we calculate the streaming particle flux according to Eq. (2) by integrating its source, $C^s + \Sigma$, over space. Finally, the streaming particle distribution function f^s is determined from the quotient of the net particle flux and a geometric estimate of the flux factor. The diffusion source will turn out to have an additional weak dependence on f^s . Thus, iterations or information from past time steps will be used in the above sequence to reach a consistent solution.

2.1. Application to radiative transfer of massless particles

As our target application is neutrino transport in core collapse supernovae, we develop and test the IDSA using the example of the $O(v/c)$ Boltzmann equation in spherical symmetry (Lindquist 1966; Castor 1972; Mezzacappa & Bruenn 1993),

$$\begin{aligned} \frac{df}{cdt} + \mu \frac{\partial f}{\partial r} + \left[\mu \left(\frac{d \ln \rho}{cdt} + \frac{3v}{cr} \right) + \frac{1}{r} \right] (1 - \mu^2) \frac{\partial f}{\partial \mu} \\ + \left[\mu^2 \left(\frac{d \ln \rho}{cdt} + \frac{3v}{cr} \right) - \frac{v}{cr} \right] E \frac{\partial f}{\partial E} \\ = j(1 - f) - \chi f + \frac{E^2}{c(hc)^3} \\ \times \left[(1 - f) \int R f' d\mu' - f \int R (1 - f') d\mu' \right]. \quad (3) \end{aligned}$$

This transport equation describes the propagation of massless fermions at the speed of light, c , with respect to a compressible background matter having a rest mass density ρ . The particle distribution function $f(t, r, \mu, E)$ depends on the time, t , radius, r , and the momentum phase space spanned by the angle cosine, μ , of the particle propagation direction with respect to the radius and the particle energy, E . The momentum phase space variables are measured in the frame comoving with the background matter, which moves with velocity v with respect to the laboratory frame. We denote the Lagrangian time derivative in the comoving frame by df/dt . Note that the derivatives $\partial f/\partial \mu$ and $\partial f/\partial E$ in Eq. (3) are also understood to be taken comoving with a fluid element. The particle density is given by an integration of the distribution function over the momentum phase space, $n(t, r) = 4\pi/(hc)^3 \int f(t, r, \mu, E) E^2 dE d\mu$, where h denotes Planck's constant. On the right hand side, we include a particle emissivity, j , and a particle absorptivity, χ , as well as an isoenergetic scattering kernel, R . We write out all blocking factors $(1 - f)$ in Eq. (3) to ease the identification of in-scattering and out-scattering terms. The shorthand notation f' refers to $f(t, r, \mu', E)$, where μ' is the angle cosine over which the integration is performed. For the present state of our approximation we neglect inelastic scattering.

2.2. Trapped particles

We separate the particles described by the distribution function $f = f^t + f^s$ in Eq. (3) into a 'trapped particle' component, described by a distribution function f^t , and a 'streaming particle' component, described by a distribution function f^s . We assume that the two components evolve separately according to Eq. (3), coupled only by

an as yet unspecified source function Σ which converts trapped particles into streaming ones and vice versa. In this subsection we discuss the evolution equation of the trapped particle component,

$$\begin{aligned} \frac{df^t}{cdt} + \mu \frac{\partial f^t}{\partial r} + \left[\mu \left(\frac{d \ln \rho}{cdt} + \frac{3v}{cr} \right) + \frac{1}{r} \right] (1 - \mu^2) \frac{\partial f^t}{\partial \mu} \\ + \left[\mu^2 \left(\frac{d \ln \rho}{cdt} + \frac{3v}{cr} \right) - \frac{v}{cr} \right] E \frac{\partial f^t}{\partial E} \\ = j - (j + \chi) f^t - \Sigma \\ + \frac{E^2}{c(hc)^3} \left[\int R f^{t'} d\mu' - f^t \int R d\mu' \right]. \quad (4) \end{aligned}$$

We assume that the distribution of the trapped particle component, $f^t = f^t(t, r, E)$, and the source function, Σ , are isotropic. The angular integration of Eq. (4) then reduces to

$$\frac{df^t}{cdt} + \frac{1}{3} \frac{d \ln \rho}{cdt} E \frac{\partial f^t}{\partial E} = j - (j + \chi) f^t - \Sigma. \quad (5)$$

However, even if we are now steering towards the hydrodynamic limit, the evolution of the trapped particle distribution function in our approximation should at least reproduce the correct diffusion limit. The physical understanding of diffusion relies on fast-moving particles with a very short transport mean free path (see the derivation of the diffusion limit, Eq. (39), in Appendix A). The divergence of the small net particle flux leads to a slow drain (or replenishment) of particles in a fluid element. In order to accomodate this diffusive drain (or replenishment) of trapped particles in Eq. (5), we have to implement it through the so far unspecified source term Σ . In the framework of our approximation, trapped particles are converted to streaming ones (or vice versa) at the same rate diffusion would drain (or replenish) particles in the fluid element. A comparison of Eq. (5) with Eq. (39) in Appendix A suggests the following diffusion source,

$$\Sigma = \frac{1}{r^2} \frac{\partial}{\partial r} \left(\frac{-r^2}{3(j + \chi + \phi)} \frac{\partial f^t}{\partial r} \right) + (j + \chi) \frac{1}{2} \int f^s d\mu. \quad (6)$$

Isoenergetic scattering enters Eq. (5) only via its opacity ϕ in the expression for the transport mean free path $\lambda = 1/(j + \chi + \phi)$ that determines the flux in Eq. (6) (see Appendix A). The additional term $(j + \chi)/2 \int f^s d\mu$ accounts for the absorption of streaming particles in matter. Its necessity is best understood with the help of Fig. (1). Shown are the different particle fluxes that relate to one fluid element. The fluid element contains both matter and trapped particles. They interact by the emissivity j and absorption $(j + \chi) f^t$ (vertical arrows). The radiation particles leaving the fluid element will convert into streaming particles at the rate Σ (upper horizontal arrow). We do not include the possibility of a direct emission of matter into the streaming particle component because this process is more easily accounted for by a high conversion rate Σ of trapped particles. On the other hand, we account for streaming particles that are absorbed by matter as represented by the arrow denoted by $(j + \chi) f^s$ in Fig. (1). In the diffusion limit, the net particle exchange of the fluid element with its

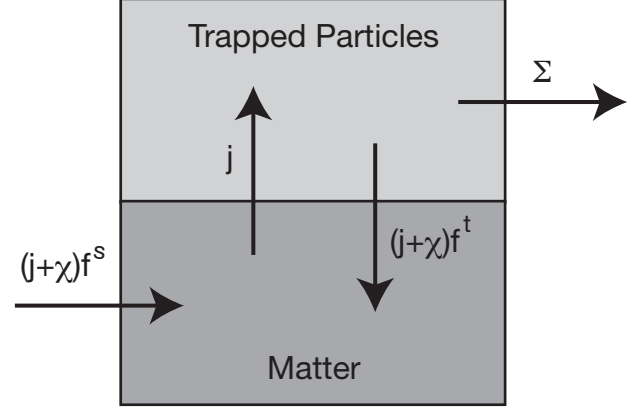


FIG. 1.— The shaded box schematically represents a fluid element in the diffusion source approximation. It contains matter (lower part) and trapped radiation particles (upper part). The interaction with other fluid elements can exclusively occur by the exchange of streaming particles or the combined hydrodynamics of the matter and trapped particles. Hence, streaming particles can be absorbed in matter at the rate $(j + \chi) f^s$ and trapped particles are converted to streaming particles at the rate Σ . Within the fluid element, matter emits trapped particles at the rate j and absorbs trapped particles at the rate $(j + \chi) f^t$. The emissivity in the absorption term originates from the identity $j(1 - f) - \chi f = j - (j + \chi) f$, which hides the Pauli blocking factor in the absorption term.

environment, $\Sigma - (j + \chi)/2 \int f^s d\mu$, must correspond to the diffusion term in Eq. (39). This is the case for our choice of Σ in Eq. (6).

If the above scheme is applied in a more transparent regime where the diffusion approximation does not hold, the diffusion source in Eq. (6) may become arbitrarily large. This would be inconsistent with the particle fluxes drawn in Fig. (1) because over a long time the diffusion source can not exceed the emissivity of trapped particles without creating an unphysical deficit in trapped particles. Instead, we would like the trapped particle component to drop to zero and stay zero in the limit of long mean free paths. This is achieved if we limit the diffusion source in Eq. (6) to $\Sigma \leq j$. If the diffusion source and emissivity reach equality, the matter absorptivity $-(j + \chi) f^t$ removes remaining trapped particles while all newly emitted ones are directly converted to streaming particles that escape the fluid element. With this limit imposed, the net interaction of particles with matter in Fig. (1) has the correct limit for large mean free paths, $j - (j + \chi) f^s$.

The search for a lower bound to the diffusion source is less straight-forward. In principle, a negative Σ can not be physically excluded. It corresponds to streaming particles that become trapped in a region of large opacity and low absorptivity. A limit corresponding to the restriction $f^t \leq 1$ would suggest $\Sigma \geq -\chi$. However, $f^t = 1$ can be an excessively large particle density compared to the physically expected value. Much more stable and more accurate results were obtained by the requirement that $f^t \leq j/(j + \chi)$, where $j/(j + \chi)$ represents the equilibrium distribution function. If one considers this condition for the particle fluxes in Fig. (1) this leads to the simple requirement $\Sigma \geq 0$. Hence, the net absorption of particles in a fluid element can not exceed $(j + \chi) f^s$. The diffusion source from Eq. (6) then

becomes

$$\Sigma = \min \left\{ \max \left[\alpha + (j + \chi) \frac{1}{2} \int f^s d\mu, 0 \right], j \right\}$$

$$\alpha = \frac{1}{r^2} \frac{\partial}{\partial r} \left(\frac{-r^2}{3(j + \chi + \phi)} \frac{\partial f^t}{\partial r} \right). \quad (7)$$

Assuming that the streaming particle density $1/2 \int f^s d\mu$ was known from the considerations described in the following subsection, Eq. (5) can be used to calculate the evolution of the trapped particle component consistently with the diffusion source specified in Eq. (7).

2.3. Streaming particles

The evolution equation for the streaming particle component consists of all terms in Eq. (3) that have not been considered in the evolution equation (4) for the trapped particles. As mentioned above, we neglect direct scattering from the trapped component into the streaming component and vice versa. That is

$$\begin{aligned} \frac{df^s}{cdt} + \mu \frac{\partial f^s}{\partial r} + \left[\mu \left(\frac{d \ln \rho}{cdt} + \frac{3v}{cr} \right) + \frac{1}{r} \right] (1 - \mu^2) \frac{\partial f^s}{\partial \mu} \\ + \left[\mu^2 \left(\frac{d \ln \rho}{cdt} + \frac{3v}{cr} \right) - \frac{v}{cr} \right] E \frac{\partial f^s}{\partial E} = -(j + \chi) f^s \\ + \Sigma + \frac{E^2}{c(hc)^3} \left[\int R f^{s'} d\mu' - f^s \int R d\mu' \right]. \end{aligned} \quad (8)$$

For the evolution of streaming particles we neglect the scattering integrals on the right hand side of Eq. (8), because the streaming particle density is designed to be small compared to the trapped particle density in regions where the scattering rate dominates the interactions. The weak coupling between streaming particles and the background matter in more transparent regimes where the streaming particle component becomes large makes an inertial laboratory frame more convenient for the solution of Eq. (8) than the frame comoving with the fluid. One may simply substitute the conditions $d \ln \rho / cdt = 0$ and $v = 0$ for a static background in Eq. (8) to find the streaming particle evolution equation in the laboratory frame:

$$\frac{\partial \hat{f}^s}{c \partial t} + \hat{\mu} \frac{\partial \hat{f}^s}{\partial r} + \frac{1}{r} (1 - \hat{\mu}^2) \frac{\partial \hat{f}^s}{\partial \hat{\mu}} = -(\hat{j} + \hat{\chi}) \hat{f}^s + \hat{\Sigma}. \quad (9)$$

Note that the quantities carrying a hat now are measured in the laboratory frame. In this frame, the particle energy is a constant of motion. The cumbersome energy derivatives of the distribution function in Eq. (8) are avoided, but some quantities require Lorentz transformations between the comoving and laboratory frames.

In contrast to the full Boltzmann equation (3), the source term on the right hand side couples only weakly to the particle distribution function \hat{f}^s . In the diffusive domain, the angle integrated term $-(\hat{j} + \hat{\chi}) \hat{f}^s$ cancels to a large extent with the corresponding contribution to $\hat{\Sigma}$ as defined in Eq. (7). In the free streaming domain, the emissivity \hat{j} and opacity $\hat{\chi}$ are assumed to be small. Depending on the application, there might be various suitable approaches to solve Eq. (9). Here, we will proceed with a stationary-state approximation. If we assume

that the fluxes of free streaming particles reach stationary values much faster than the dynamical time scale of interest, we can drop the time-derivative in the first term in Eq. (9). If the source on the right hand side is assumed to be known from a consistent solution of Eqs. (5) and (7), the integration of Eq. (9) over angles leads to a Poisson equation for a potential ψ , whose gradient represents the particle flux:

$$\begin{aligned} \frac{\partial \psi}{\partial r} &= \frac{1}{2} \int \hat{f}^s \hat{\mu} d\hat{\mu} \\ \frac{1}{r^2} \frac{\partial}{\partial r} \left(r^2 \frac{\partial \psi}{\partial r} \right) &= \frac{1}{2} \int \left[-(\hat{j} + \hat{\chi}) \hat{f}^s + \hat{\Sigma} \right] d\hat{\mu}. \end{aligned} \quad (10)$$

In the end, we are interested in the streaming particle density rather than flux. Both quantities are related by the flux factor. It is a very challenging problem to calculate an accurate flux factor. However, Bruenn in (Liebendörfer et al. 2004) suggested a simple and very successful approximation based on the assumption that all particles of a given energy are isotropically emitted at their corresponding scattering sphere. This leads to the additional relation

$$\frac{1}{2} \int \hat{f}^s(E) d\hat{\mu} = \frac{2 \frac{\partial \psi}{\partial r}(E)}{1 + \sqrt{1 - \left(\frac{R_\nu(E)}{\max(r, R_\nu(E))} \right)^2}}, \quad (11)$$

where $R_\nu(E)$ is the radius of the monochromatic scattering sphere that depends on the particle energy E .

In order to solve for both trapped and streaming particle components, we have to Lorentz-transform quantities between the comoving and laboratory frames. The source of Eq. (10) in the laboratory frame is related to the comoving frame by

$$\begin{aligned} \frac{1}{2} \int \left[-(\hat{j} + \hat{\chi}) \hat{f}^s + \hat{\Sigma} \right] d\hat{\mu} \hat{E}^2 d\hat{E} \\ = \frac{1}{2} \int \left[-(j + \chi) f^s + \Sigma \right] d\mu E^2 dE. \end{aligned} \quad (12)$$

Here we used the fact that the source is isotropic in the comoving frame together with the relations $d\hat{\mu} \hat{E} d\hat{E} = d\mu E dE$, $\hat{E} = \gamma(1 + \mu v/c)E$ and $\hat{j} \hat{E} = jE$ (Mihalas & Weibel Mihalas 1984), where $\gamma = 1/\sqrt{1 - (v/c)^2}$ is the Lorentz factor. On the other hand, the streaming particle contribution to Eq. (7) in the comoving frame is related to the solution of Eq. (10) in the laboratory frame by

$$\begin{aligned} \frac{1}{2} \int f^s d\mu E^2 dE &= \frac{1}{2} \int \hat{f}^s \gamma (1 - \hat{\mu} v/c) d\hat{\mu} \hat{E}^2 d\hat{E} \\ &= \gamma \left(\frac{1}{2} \int \hat{f}^s d\hat{\mu} - \frac{v}{c} \frac{\partial \psi}{\partial r} \right) \hat{E}^2 d\hat{E}, \end{aligned} \quad (13)$$

where the first term is given in Eq. (11). In $O(v/c)$ we may neglect the factor γ .

Hence, as soon as the evolution of the trapped particle component according to Eq. (5) has determined the source in Eq. (7), one can transform it to the laboratory frame by Eq. (12). Then one determines the stationary-state streaming particle flux and density based on Eqs. (10) and (11) in the laboratory frame. The resulting streaming particle density is transformed back to the comoving frame by Eq. (13). In this form it can be used for the next iteration or time step in Eq. (7).

2.4. Coupling with hydrodynamics

The evolution of the trapped particle component in Eqs. (5) and (7) and the stationary-state limit of the streaming particle component in Eqs. (10) and (11) must be coupled with the dynamics of the background matter. We assume that the dynamics of the background matter is well described by the conservation laws of hydrodynamics,

$$\frac{\partial}{\partial t}U + \frac{\partial}{r^2 \partial r}(r^2 F) = 0, \quad (14)$$

where U is a vector of primitive variables and F a vector of fluxes. We rewrite the evolution equation (5) for the trapped particle component with an Eulerian time derivative and use the continuity equation to substitute the $d \ln \rho / dt$ term by the velocity divergence,

$$\begin{aligned} \frac{\partial f^t}{\partial t} + \frac{\partial}{r^2 \partial r} \left(r^2 \frac{v}{c} f^t \right) - \frac{\partial}{r^2 \partial r} \left(r^2 \frac{v}{c} \right) \frac{\partial (E^3 f^t)}{3 E^2 \partial E} \\ = j - (j + \chi) f^t - \Sigma. \end{aligned} \quad (15)$$

One could now merge the hydrodynamical update on the left hand side of Eq. (15) with the conservation law in Eq. (14). However, if the dynamics of the background matter requires a large-scale numerical simulation and if there are many particle species, the required memory and CPU time to store and advect all these quantities can easily exceed the capacity of the available hardware. In our supernova application, for example, we need in three dimensions a vector U of 6 entries to describe the hydrodynamics as detailed below. The neutrino transport involves 2-4 neutrino species (ν_e , $\bar{\nu}_e$, $\nu_{\mu/\tau}$, $\bar{\nu}_{\mu/\tau}$) with at least 12 entries per species to sample the different neutrino energies E in $f^t(t, r, E)$.

If the characteristic time scale of local reactions between the transported particle species is faster than the diffusion time scale, one can use equilibrium conditions to reduce the number of primitive variables necessary to describe the distribution functions of trapped particles. In the supernova model, for example, we can approximate the spectrum by a thermal spectrum. Note, that this assumption is only made for the *trapped* particles within a fluid element. The streaming particles, which communicate *between* fluid elements, keep their detailed spectral information. Our scheme should therefore not be confused with a 'grey' scheme that may additionally assume a predefined energy-spectrum for the particle exchange between fluid elements. We characterise the thermal equilibrium by a particle number fraction, Y^t , and a particle mean specific energy, Z^t ,

$$\begin{aligned} Y^t &= \frac{m_b}{\rho} \frac{4\pi}{(hc)^3} \int f^t E^2 dE d\mu \\ Z^t &= \frac{m_b}{\rho} \frac{4\pi}{(hc)^3} \int f^t E^3 dE d\mu, \end{aligned} \quad (16)$$

where m_b is a constant relating a particle number to the rest mass of the background matter (in our application it is the baryon mass).

The corresponding energy integrals performed on Eq. (15) lead to evolution equations for Y^t and Z^t ,

$$\frac{\partial}{\partial t}(\rho Y^t) + \frac{\partial}{r^2 \partial r}(r^2 v \rho Y^t)$$

$$\begin{aligned} &= m_b \frac{4\pi c}{(hc)^3} \int \left[j - (j + \chi) f^t - \frac{1}{2} \int \Sigma d\mu \right] E^2 dE \\ &\frac{\partial}{\partial t}(\rho Z^t) + \frac{\partial}{r^2 \partial r}(r^2 v \rho Z^t) + \frac{\partial}{r^2 \partial r}(r^2 v) \frac{\rho Z^t}{3} \\ &= m_b \frac{4\pi c}{(hc)^3} \int [j - (j + \chi) f^t - \Sigma] E^3 dE. \end{aligned}$$

The equation for Z^t corresponds to an energy equation with a pdV term for the radiation pressure $\rho Z^t/3$ on the left hand side. Analogously to an entropy equation it can be cast into a conservative form for the evolution of $(\rho Z^t)^{3/4}$. Hence, one can solve the advective part of Eq. (15) together with the hydrodynamics conservation law (14) based on the following primitive variables:

$$U = \begin{pmatrix} \rho \\ \rho v \\ \rho \left(e + \frac{1}{2} v^2 \right) \\ \rho Y_e^t \\ \rho Y_l^t \\ (\rho Z_l^t)^{\frac{3}{4}} \end{pmatrix}, \quad F = \begin{pmatrix} v \rho \\ v \rho v + p \\ v \rho \left(e + \frac{1}{2} v^2 + \frac{p}{\rho} \right) \\ v \rho Y_e^t \\ v \rho Y_l^t \\ v (\rho Z_l^t)^{\frac{3}{4}} \end{pmatrix}, \quad (17)$$

where p is the fluid pressure, e the fluid specific internal energy and Y_e the electron fraction. The index l labels different species of trapped particles.

As the distribution function of trapped particles in thermal equilibrium, $f_l^t(E) = \{\exp[\beta_l(E - \mu_l)] + 1\}^{-1}$, has two free parameters β_l and μ_l , it can be reconstructed so that Eq. (16) is fulfilled for the new values of Y_l^t and Z_l^t . Then, the remaining update of the trapped particle distribution in Eq. (15) is given by

$$\frac{\partial f_l^t}{\partial t} = j_l - (j_l + \chi_l) f_l^t - \Sigma_l. \quad (18)$$

This equation also determines the net interaction rates, $s_l = j_l - (j_l + \chi_l)(f_l^t + f_l^s)$, between matter and the radiation particles, which leads to the following changes of the electron fraction and internal specific energy:

$$s_l = \frac{\partial f_l^t}{\partial t} + \Sigma_l - (j_l + \chi_l) \frac{1}{2} \int f_l^s d\mu \quad (19)$$

$$\frac{\partial Y_e}{\partial t} = -\frac{m_b}{\rho} \frac{4\pi c}{(hc)^3} \int (s_{\nu_e} - s_{\bar{\nu}_e}) E^2 dE \quad (20)$$

$$\frac{\partial e}{\partial t} = -\frac{m_b}{\rho} \frac{4\pi c}{(hc)^3} \int (s_{\nu_e} + s_{\bar{\nu}_e}) E^3 dE. \quad (21)$$

The changes in the matter electron fraction and specific energy feed back into the emissivity and absorptivity used in Eq. (18). Once a consistent solution has been found, Eq. (18) allows updates of the trapped particle fraction, of the trapped particle specific energy, and of the matter velocity, which is subject to radiation pressure.

$$\frac{\partial Y_l^t}{\partial t} = \frac{m_b}{\rho} \frac{4\pi c}{(hc)^3} \int \frac{\partial f_l^t}{\partial t} E^2 dE \quad (22)$$

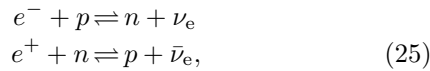
$$\frac{\partial Z_l^t}{\partial t} = \frac{m_b}{\rho} \frac{4\pi c}{(hc)^3} \int \frac{\partial f_l^t}{\partial t} E^3 dE \quad (23)$$

$$\frac{\partial v}{\partial t} = -\frac{1}{\rho} \frac{\partial}{\partial r} \left(\frac{\rho Z_l^t}{3 m_b} \right). \quad (24)$$

Finally, the cycle of updates is completed by the solution of Eqs. (10) and (11) for the distribution function f^s for streaming particles based on the sources determined in Eqs. (18) and (7). Details on the finite differencing of our implementation of the IDSA are given in Appendix B.

3. VERIFICATION FOR SPHERICALLY SYMMETRIC SUPERNOVA MODELS

We implement the IDSA in the hydrodynamics code Agile (Liebendörfer et al. 2002). For the evaluation of the radiative transfer approximations, we run the simulations in the Newtonian limit and include only electron flavour neutrinos. Their dominant emission and absorption reactions are



where e^- , e^+ , ν_e , $\bar{\nu}_e$ refer to electrons, positrons, electron neutrinos and electron antineutrinos, respectively, that interact with protons, p , and neutrons n . The opacities in our example are given by isoenergetic scattering on nucleons and nuclei. All weak interactions are implemented as described in (Bruenn 1985). The thermodynamical state of matter as a function of density, ρ , temperature, T , and electron fraction, Y_e , is calculated by the Lattimer-Swesty equation of state (Lattimer & Swesty 1991).

Very simple and efficient approximations to treat the deleptonisation in the collapse phase have been suggested and evaluated in an earlier paper (Liebendörfer 2005). Here we concentrate on the postbounce phase, which is more difficult to capture with neutrino physics approximations. The neutrinos not only leak out, but they also interact at distant locations and feed back into the hydrodynamics by their transfer of lepton number and energy. Due to the as yet restricted input physics, we base our first comparison on model N13 in (Liebendörfer et al. 2005), which we have repeated with the most recent code version to obtain perfect consistency in all parts that are not related to the neutrino transport. The additional neutrino-electron scattering and pair creation rates, which are included in model N13, do not significantly contribute to the electron flavour neutrino transport in the postbounce phase. In order to keep the approximation as simple as possible, we additionally neglect the transformations between comoving and laboratory frames in our current implementation.

We start with the verification of the description of the trapped particle component. The trapped particle distribution function is assumed to be thermal and is parameterised by the two parameters inverse temperature, β , and the particle degeneracy parameter, $\mu/(kT)$. They are chosen such that Eq. (16) is fulfilled. In Fig. 2 we compare these parameters to the temperature of matter and to the equilibrium degeneracy parameter determined by reactions (25). We find as expected that the neutrino distribution function of a reference simulation with Boltzmann neutrino transport is very well described by the parameterisation in regimes where the neutrinos are trapped and thermal and weak equilibrium are good approximations. Deviations are visible where the neutrinos start to decouple from matter. The IDSA leads to decreasing trapped particle abundances in this transition regime as more and more particles change from

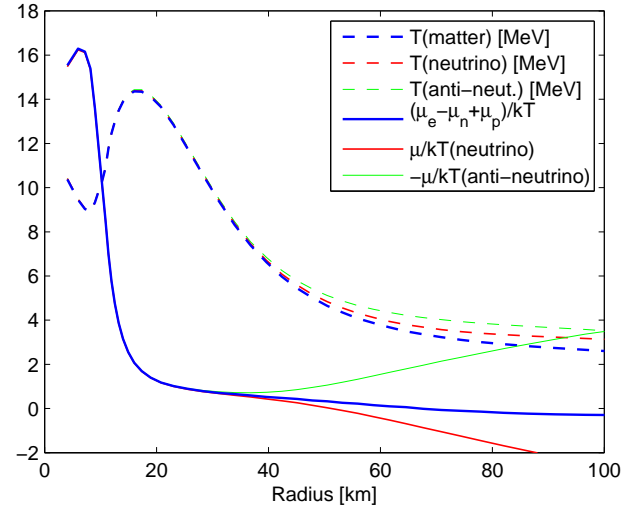


FIG. 2.— Neutrino temperature and degeneracy parameters resulting from the application of Eq. (16) at a typical time of 150 ms after bounce. As indicated in the legend, the solid lines show the degeneracy of the particles involved in Eq. (25) together with the (anti-)neutrino degeneracy parameters. The dashed lines show the matter temperature together with the (anti-)neutrino temperature parameters.

the trapped particle component to the streaming particle component. This is visible in the decreasing chemical potentials at radii larger than 40 km. The temperature parameter of the remaining trapped particle component is slightly larger than the temperature of the matter.

This decoupling of particles from opaque matter is an important feature that needs to be handled by a radiative transfer algorithm. Since the IDSA treats this transition by a gradual conversion of ‘trapped particles’ to ‘streaming particles’, we can compare the sum of the trapped particle and streaming particle densities with the total particle density in a reference simulation that solves the Boltzmann equation. Fig. 3 shows this comparison for a typical time slice at 150 ms after bounce. Because the trapped particle distribution function in Eq. (16) is characterised by the particle abundance and mean energy, we select these two quantities for the comparison. Panel (a) shows how the trapped and streaming particle abundances overlap and add up to a reasonable total particle abundance. Panel (b) shows similar agreement in the particle mean energies. Although the results agree very well in general, we also note that the deviations are largest around 50 km radius. Fig. 2 indicates that this is exactly in the difficult regime where the neutrinos decouple from matter. The less relevant deviations at radii larger than 220 km stem from the Doppler energy shift at the shock front, that is not present in the IDSA data, because the transformation between the laboratory and comoving frames has been neglected.

We can analyse the discrepancies further by looking at the particle spectra in the different regimes. The panels on the left hand side of Fig. 4 show neutrino spectra, while the panels on the right hand side show antineutrino spectra. The spectra in panels (a) and (b) are taken at 40 km radius from the time slice at 150 ms after bounce. One can immediately see that the trapped neutrino component (dashed lines) dominates over the

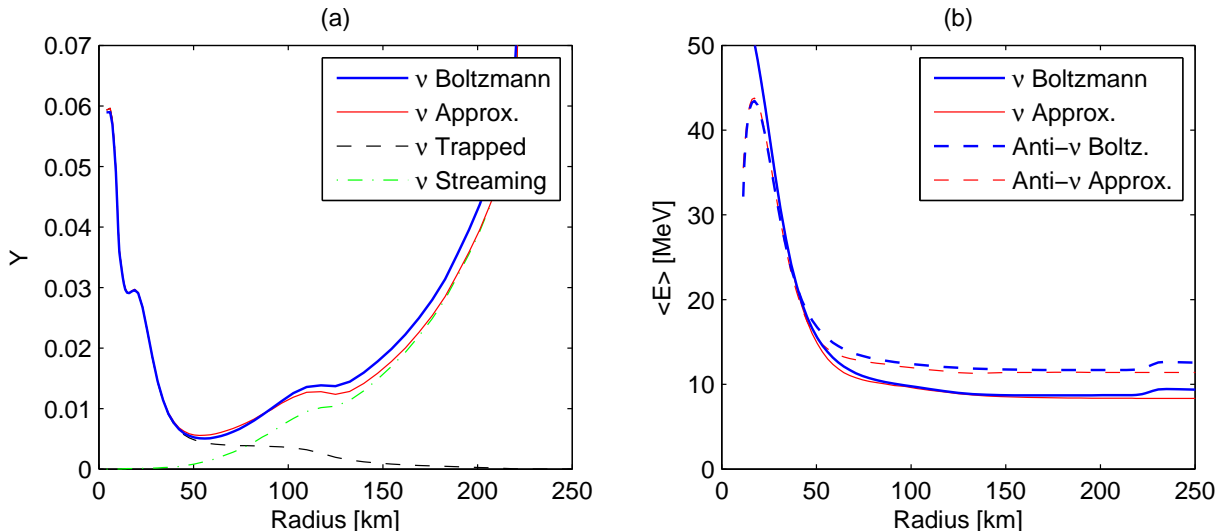


FIG. 3.— Panel (a) shows neutrino abundances as a function of radius at a typical postbounce time of 150 ms. The thick solid line shows the neutrino abundance in the reference simulation with Boltzmann transport. The application of the IDSA leads to a trapped neutrino abundance (dashed line) and a streaming neutrino abundance (dash-dotted line). They sum up to the total neutrino abundance (thin solid line), which is comparable to the Boltzmann result. Graph (b) demonstrates that also the neutrino mean energies between the reference model (thick lines) and the IDSA (thin lines) agree nicely.

streaming particle component (dash-dotted lines). The sum of both (thin solid line) matches well with the reference solution (thick solid line). At these conditions the spectrum of the neutrinos is very accurately represented by the IDSA, while small differences become visible in the antineutrino spectra. The spectra match well, because the thermal distribution function used for the trapped neutrino component is still a good approximation at the border of the neutrino-opaque regime. Panels (c) and (d) show the same quantities further out, where the trapped and streaming particle abundances reach about the same value (i.e. at ~ 80 km radius). The particle abundances again match well with the reference data, but the neutrino spectra in the IDSA peak at lower energies than in the reference simulation. This is consistent with the findings above in Fig. 3. The reason is that the assumption of a thermal spectrum for the trapped particle component starts to become inaccurate at 80 km radius, while the trapped particle component still makes a significant contribution of $\sim 50\%$ to the total abundance. The inaccuracy of a thermal spectrum in the semi-transparent regime is well-documented in the supernova literature (e.g. Myra & Burrows (1990)) and appears most dramatic if presented on logarithmic axes. We prefer a linear axis where the total particle abundance, or deviations between abundances, are proportional to the enclosed area between the lines. At a radius of 160 km the streaming particle component dominates over the trapped particle component as shown in panels (e) and (f). The comparison of the spectra shows more accurate agreement because the streaming particle component keeps its full spectral information in the IDSA. Some deviations in the abundances are visible. They are most likely an effect of the approximations in the decoupling regime and demonstrate the limitations of the IDSA.

At this stage we are curious, how much accuracy was lost by the decision to parameterise the trapped particle component by a thermal distribution function. In or-

der to test this, we developed an alternative version that takes deviations from the thermal trapped particle spectrum into account. The details of this test approach are described in Eq. (55) in Appendix B. The resulting spectra of this more complicated version are shown in Fig. 5. Now the reference spectra are perfectly matched by the IDSA results at 40 km radius and for the antineutrinos also at 160 km radius. Even in the difficult regime at 80 km radius the spectral shapes agree very nicely with the reference. But new deviations appear this time in the particle abundances, which are somewhat smaller in the IDSA data than in the reference data. We conclude from these comparisons that the results of the IDSA are in qualitatively robust agreement with the reference data, but inaccuracies of 10 – 20% are likely to be present in the details of the distribution function and are difficult to remove by simple upgrades. In order to become able to better distinguish the systematic errors from the accidental errors, we include both the normal and the spectral version of the IDSA in the following comparisons with the reference data.

Once the trapped and streaming particle components are specified we investigate the resulting net heating and cooling rates from neutrino absorption and emission. Fig. 6 shows the energy exchange between neutrinos and matter separately for the neutrinos (solid lines) and antineutrinos (dashed lines). This comparison has to be performed and interpreted very carefully, because the matter conditions are partially in equilibrium with the transported particles. Even minor deviations from the stationary-state equilibrium at a restart of the calculation may lead to large transient corrections in the exchange rates. Hence, we let the hydrodynamics, the reference simulation and the IDSA solution evolve after restart at 150 ms postbounce until the stationary-state is achieved in both cases. The agreement of the IDSA (lines labelled with ‘Approx.’ and ‘Spectra’) with the reference simulation (line labelled with ‘Boltzmann’) is excellent in

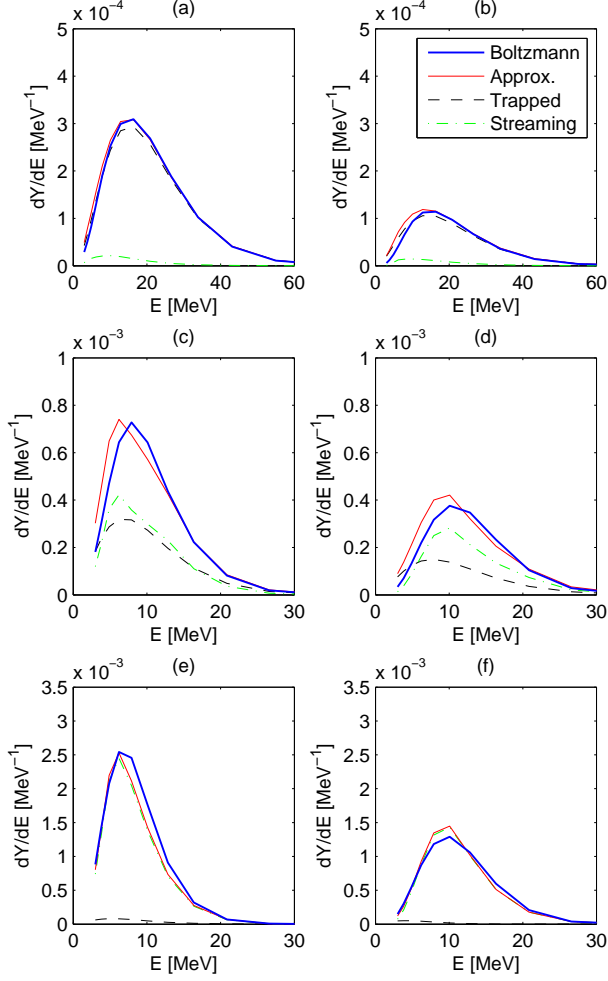


FIG. 4.— Particle spectra for the trapped particle component (dashed line), the streaming particle component (dash-dotted line), their sum (thin solid line) and the reference simulation (thick solid line) at selected radii. Panels (a) and (b) show spectra at 40 km radius, panels (c) and (d) at 80 km radius and panels (e) and (f) at 160 km radius. The panels on the left hand side (a,c,e) show neutrino spectra while the panels on the right hand side (b,d,f) show antineutrino spectra.

the heating region at radii larger than 120 km. Differences of up to 30% can be seen in the cooling rates at smaller radii in the rates for the antineutrinos (dashed lines). The IDSA with a spectral representation of the trapped particles (lines labelled with 'Spectral') performs better than the IDSA with the approximate representation of trapped particles (lines labelled with 'Approx.'). The reference simulation shows stronger cooling by neutrinos than antineutrinos at 95 km radius. This detail feature is not reproduced by either IDSA version. However, as the cooling rates are a response to an intricate dynamical equilibrium between the hydrodynamics and the quantities evolved by the transport algorithm, a simple comparison of the heating and cooling rates alone is not sufficient to predict the accuracy of a long-term evolution. In analogy, the instantaneous corrections applied to the steering wheel of a car can vary from driver to driver, but most drivers follow the trajectory of the road on the long term.

A comparison of profiles at the very early postbounce

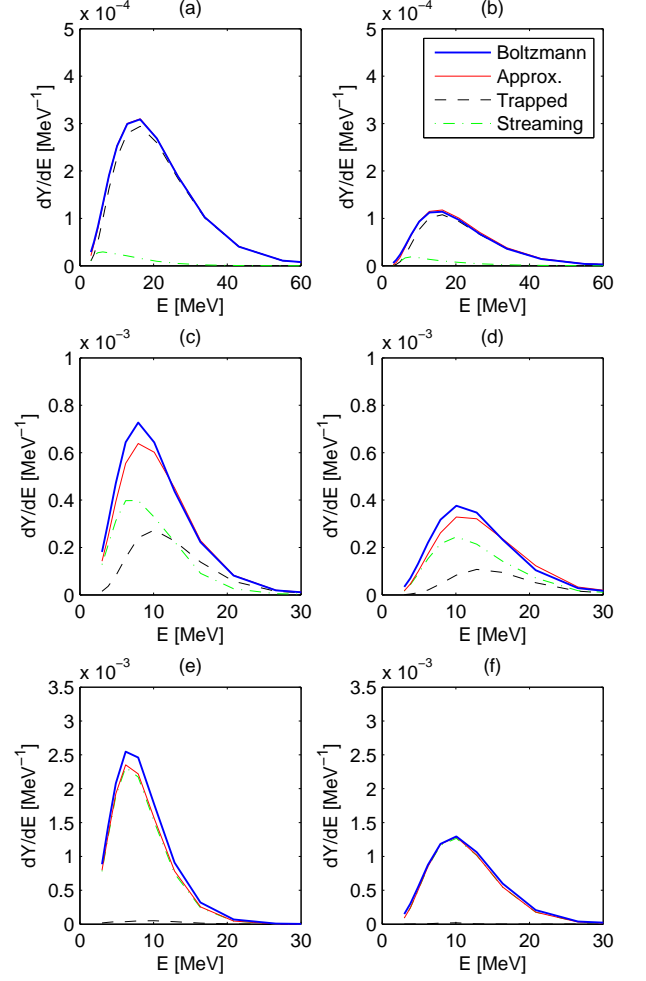


FIG. 5.— The approximate data in this figure has been calculated with a version of the IDSA where the spectral information about the trapped particle component is retained as described in Appendix B. Otherwise, the representation is the same as in Fig. 4: Panels (a) and (b) show spectra at 40 km radius, panels (c) and (d) at 80 km radius and panels (e) and (f) at 160 km radius. The panels on the left hand side (a,c,e) show neutrino spectra while the panels on the right hand side (b,d,f) show antineutrino spectra.

times of 1 and 3 ms is shown in Fig. 7. No significant deleptonisation has occurred before 1 ms after bounce, while at 3 ms after bounce the launch of the neutrino burst is reflected in a trough of the electron fraction profile and a strong decline of the entropy profile at an enclosed mass $\sim 1 M_{\odot}$. Significant differences between the IDSA and the Boltzmann solution are only visible in the electron fraction profiles.

In fact, if one defines the diffusion source as described in Eq. (7), both IDSA versions lead to an earlier and somewhat faster deleptonisation than in the Boltzmann solution. Our stationary-state assumption of the free streaming particle component implies that produced neutrinos propagate infinitely fast. This assumption is not applicable in the very early postbounce phase because the dynamical changes of the matter conditions occur on a similar time scale as the neutrino transport. This transient deviation in the deleptonisation rates during the first few milliseconds lets the models start on a different footing so that the performance of the approxi-

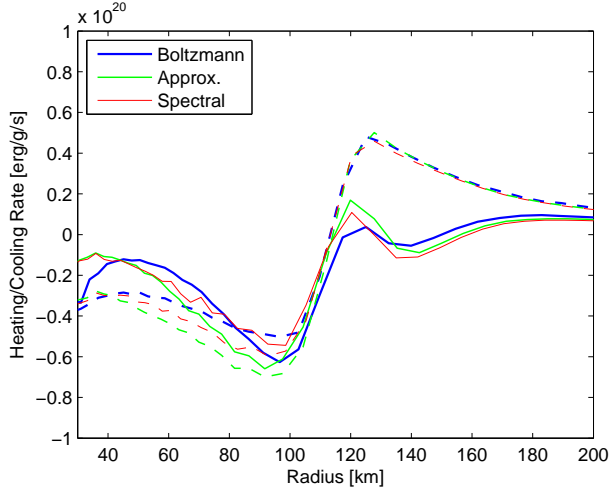


FIG. 6.— Comparison of the heating or cooling rates specific to each neutrino type at 150 ms after bounce. The solid lines show the energy exchange between neutrinos and matter. The dashed lines show the energy exchange between antineutrinos and matter. The lines labelled 'Approx.' and 'Spectral' have been calculated using the IDSA with the standard and spectral representations of the trapped particle component, respectively.

mation in the more interesting later postbounce phases becomes difficult to assess. In order to account for the neutrino propagation time in an averaged way we therefore limit the diffusion source Σ in Eq. (7) additionally by $fc/\Delta r$, where Δr is an empirically determined constant parameter that stands for a typical distance the neutrinos have to propagate until stationary-state conditions become applicable. The value $\Delta r = 15$ km leads to satisfactory results. With this, the IDSA version with the spectral treatment of the trapped particle distribution function (dash-dotted lines) leads to nice agreement with the Boltzmann results (solid lines) while the IDSA version with the two-parameter description of a thermal distribution function (dashed lines) initially deleptonises slightly slower, but excellent agreement is achieved later during the shock expansion phase. Corresponding profiles at 30 ms and 100 ms after bounce are shown in Fig. 8. The solutions based on the IDSA lead to a slightly more optimistic shock expansion, but the detailed features in the entropy and electron fraction profiles are accurately reproduced.

The shock retraction phase is shown in Fig. 9. Shown are profiles at 150 ms and 300 ms after bounce (note that now the larger shock radius belongs to the earlier time slice). The effect of neutrino heating (and hence successful neutrino transport) is clearly visible in the entropy profile. Models that implement only neutrino leakage develop a much smaller entropy that is entirely set by the heat dissipation at the shock front. In the shock retraction phase, the peak entropy is obtained at the shock front. If neutrino heating is switched on, the region of peak heating is located between the neutrinospheres and the shock radius (see Fig. 6), because the neutrino flux dilutes at larger distances and the matter density decreases in the outer layers. Figs. 8 and 9 show the negative entropy gradient between 120 km radius and the shock position that is caused by this neutrino heating. As before we obtain excellent agreement

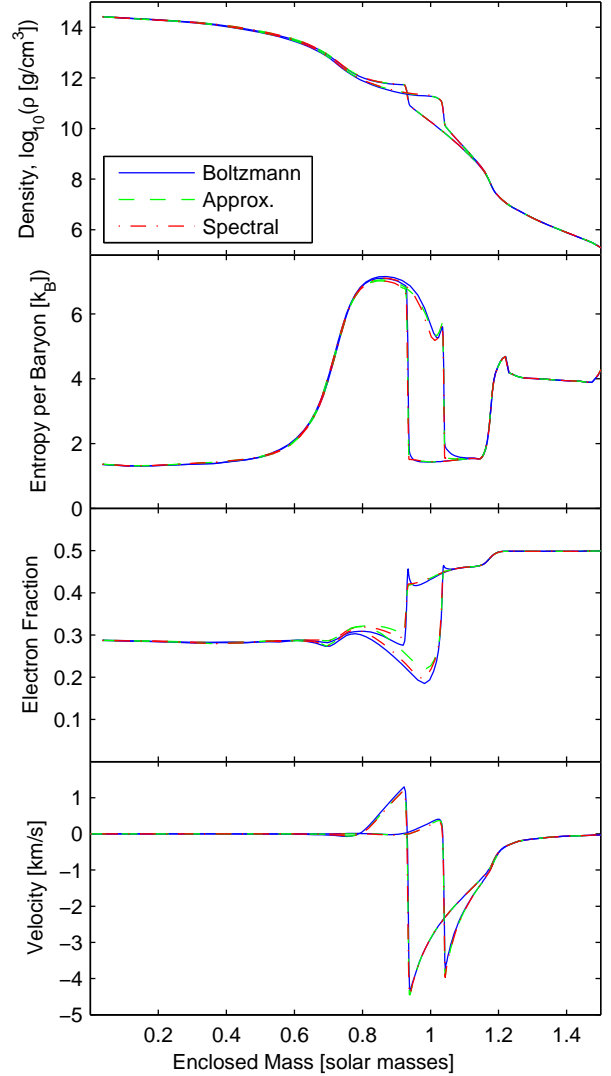


FIG. 7.— Density, entropy, electron fraction and velocity as functions of enclosed mass for a model based on Boltzmann neutrino transport (solid lines) and two models based on the IDSA. The dashed lines represent data from the IDSA using a thermal trapped particle distribution function while the dash-dotted lines represent data from the IDSA with a spectral trapped particle treatment. The comparison is shown at two different time instances: At 1 ms after bounce (lines with the shock discontinuity positioned between 0.8 and 1 M_\odot) and at 3 ms after bounce (lines with the shock discontinuity positioned between 1 and 1.2 M_\odot). Significant differences are only visible in the electron fraction profiles: The deleptonisation in the approximate model is slightly delayed.

in the diffusive regime. But the model with neutrino transport approximations starts to retract slightly earlier than the more accurate model with Boltzmann neutrino transport. This is consistent with the larger cooling rates of the IDSA model found in Fig. 6. However, the overall differences are not much larger than differences that were also found in the first comparison of two independent implementations of Boltzmann neutrino transport (Liebendörfer et al. 2005). The chances of obtaining a delayed explosion seem to be more pessimistic in the model with approximate neutrino transport.

A short overview of the comparison is given in Fig. 10 in the form of shock trajectories and neutrino lumi-

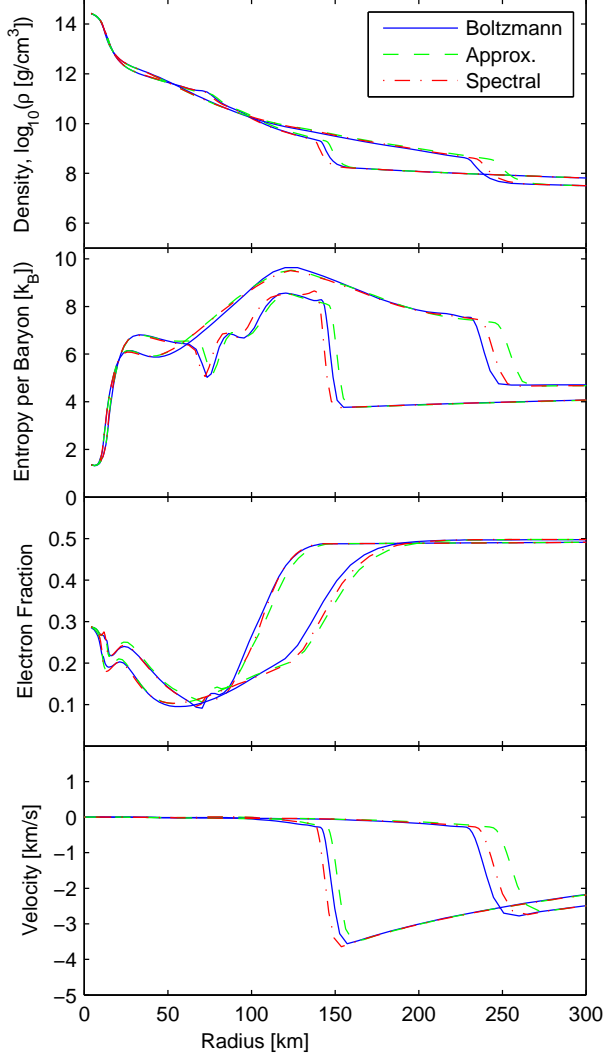


FIG. 8.— Same presentation of the data as in Fig. 7. Here, the comparison is shown at two later time instances: At 30 ms after bounce (lines with the shock discontinuity positioned at 150 km radius) and at 100 ms after bounce (lines with the shock discontinuity positioned at 250 km radius). The two IDSA solutions lead to a somewhat more optimistic shock expansion in this phase, but produce nicely detailed features in the electron fraction and entropy profiles.

nosities for the three models. Panel (a) shows the shock trajectories. As stated before, the agreement is excellent from the early postbounce phase through the shock expansion phase. The models with approximate neutrino transport initially produce a larger peak shock radius, but then compensate by a faster shock retraction. The model with the spectral treatment of the trapped particle component (dash-dotted line) is somewhat closer to the reference simulation (solid line) than the standard IDSA with the two-parameter description of the trapped particle distribution function (dashed line). Panel (b) shows the neutrino luminosities measured in the comoving frame (this distinction is only made for the Boltzmann reference results) at 500 km radius. Overall, the luminosities are in good agreement. The neutrino luminosities in the approximate models are somewhat smaller

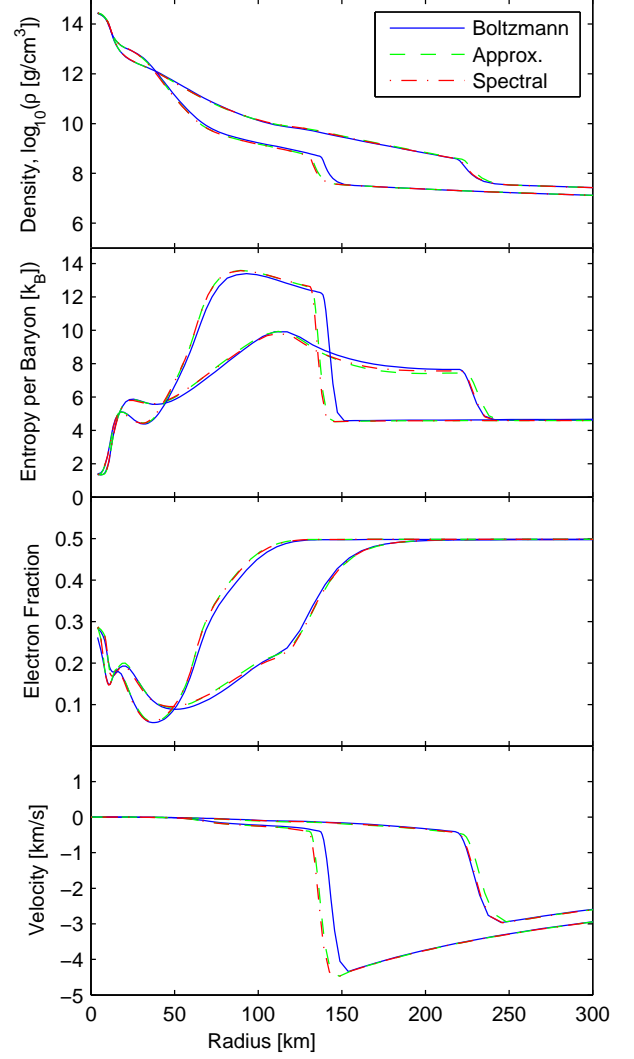


FIG. 9.— Same presentation of the data as in Fig. 7. Here, the comparison is shown at two later time instances: At 150 ms after bounce (lines with the shock discontinuity positioned at 230 km radius) and at 300 ms after bounce (lines with the shock discontinuity positioned at 150 km radius). The evolution in the diffusive domains is in good agreement, but the shock in the approximate model retracts somewhat faster than in the accurate model. With respect to a possible delayed explosion, the approximation produces the more pessimistic model.

than in the more accurate Boltzmann model.

While experimenting with different variations in the approximation scheme we found that the stationary-state luminosity in the approximate model is not a perfectly smooth function of time, which leads us to the discussion of some numerical issues related to the isotropic diffusion source approach. The numerical details of our current implementation are outlined in Appendix B. All local reaction rates and the corresponding updates of the lepton fractions and temperature are implemented in a time-implicit way. The non-local contribution from the diffusion is also unconditionally stable because the updates are ordered in such a way that each zone can use the updated distribution function of its neighbour zone in the upwind direction (with respect to the diffusion flux), while the contribution of the local distribution function

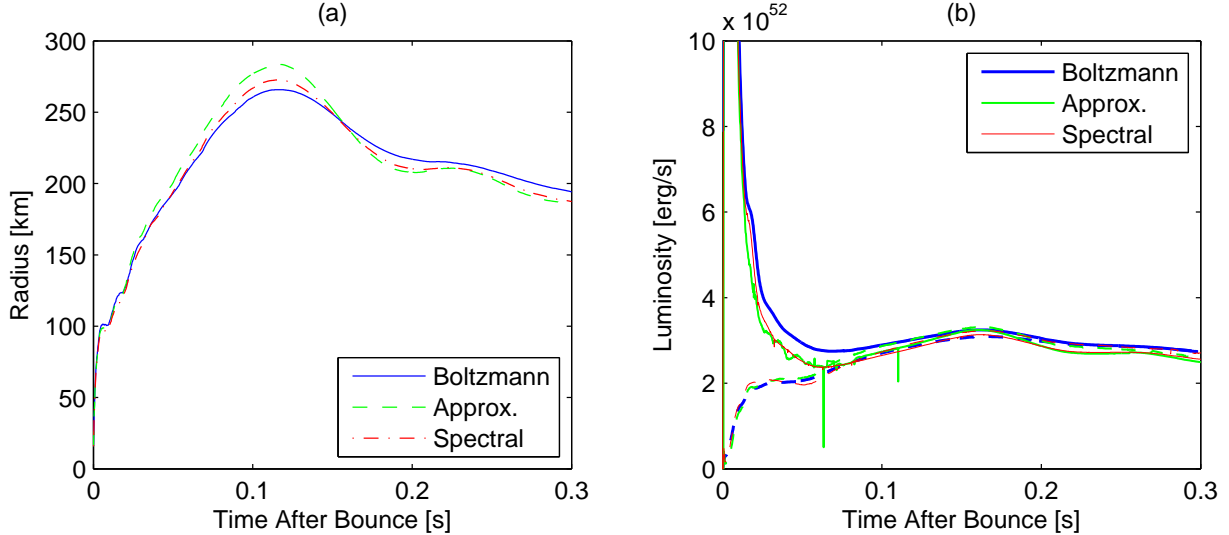


FIG. 10.— Panel (a) shows the shock position as a function of time for a model based on Boltzmann neutrino transport (solid line) and the two models using the IDSA. Both approximate models agree reasonably well with the reference model. The model based on a spectral treatment of the trapped particle distribution function (dash-dotted line) is somewhat closer than the standard IDSA approach (dashed line), but shows the same qualitative deviations of a too optimistic initial expansion and a faster shock retraction afterwards. Panel (b) shows the neutrino luminosities for the same three models. The agreement is satisfactory in general, the neutrino luminosities (thin solid lines) are generally smaller in the approximate model than in the Boltzmann model (thick solid line). The dashed lines refer to the antineutrino luminosities. Some experienced numerical difficulties with the approximate neutrino luminosities are discussed in the text.

to the diffusion term is included in the time-implicit update. However, the coupling to the stationary-state solution of the streaming particle component is operator split. It is therefore still necessary to restrict the time step to obtain a numerically stable evolution. In the diffusion limit, the operator splitting is numerically stable due to above-mentioned implicit finite differencing. In the free streaming limit, the operator splitting is numerically stable due to the absence of relevant interactions between the streaming particle component and matter. It is again the semi-transparent transition regime where the operator splitting has the highest potential for numerical instabilities. We obtain converged solutions if the time step chosen is smaller than $1 \text{ km}/c$. This corresponds to the Courant-Friedrich-Levy (CFL) limit for the speed of light or the time step limit of an explicitly finite differenced diffusion scheme where the mean free path is half the zone width, i.e. in the semi-transparent regime. If the time step chosen is larger, the stationary-state solution for the streaming particle component starts to jump from time step to time step. Rare luminosity jumps are still visible in Fig. 10b. All other variables, e.g. the lepton fractions and the temperature, do not react to these instantaneous luminosity jumps because they evolve on a slower time scale where the luminosity oscillations enter in a time-averaged manner.

In summary, we believe that the separation of particles into trapped and streaming components provides an interesting ansatz for specifically tailored simplifications of the Boltzmann transport equations. The results in Figs. 7-10 show that such a simplified description can reproduce the key features of neutrino transport in supernova models. In the diffusion limit, the results are stable and accurate. In the transition regime the time step of our current implementation is at present limited by numerical fluctuations of the stationary-state streaming particle

flux at the transition to transparent conditions. With our not thoroughly optimized code, a single time step with the IDSA is of order 100 times faster than a corresponding time step with Boltzmann neutrino transport. As the fully implicit Boltzmann transport can take about 10 times larger time steps, a full simulation with the IDSA is about an order of magnitude faster than the one with Boltzmann transport. However, this number may vary from application to application because the performance of the time-implicit Boltzmann solution does not scale favourably with an increased dimensionality and size of the computational domain. In three dimensions, we believe that simulations based on the IDSA are feasible on average size high-performance computer clusters, while simulations with comprehensive Boltzmann transport have not yet been reported to be feasible even on top-performing computer systems. A possible extension of the IDSA to multi-dimensional applications is outlined in the following section.

4. GENERALIZATION FOR MULTI-DIMENSIONAL APPLICATIONS

So far, we have discussed the IDSA only in spherical symmetry. As mentioned above, it is not the goal of this paper to develop yet another approach that works only for spherically symmetric models. Spherical symmetry is much better treated with three-flavour Boltzmann transport where the comprehensive equations of radiative transfer can consistently be solved (Rampp & Janka 2002; Thompson et al. 2003; Liebendörfer et al. 2004; Sumiyoshi et al. 2005). Hence, in this section we discuss how the scheme extends to the three-dimensional case.

The state vector U of a 3D simulation only differs from Eq. (17) by the velocity v , which becomes a vector $\vec{v} = (v_x, v_y, v_z)$. With the corresponding three directional components $i = 1 \dots 3$ in the momentum equation,

the state vector U and flux vector F become:

$$U = \begin{pmatrix} \rho \\ \rho v_i \\ \rho \left(e + \frac{1}{2}v^2\right) \\ \rho Y_e \\ \rho Y_l^t \\ (\rho Z_l^t)^{\frac{3}{4}} \end{pmatrix}, \quad F = \begin{pmatrix} \vec{\rho} \\ \vec{\rho} v_i + p \\ \vec{\rho} \left(e + \frac{1}{2}v^2 + \frac{p}{\rho}\right) \\ \vec{\rho} Y_e \\ \vec{\rho} Y_l^t \\ \vec{\rho} (\rho Z_l^t)^{\frac{3}{4}} \end{pmatrix}. \quad (26)$$

This state vector can be evolved by a standard hydrodynamics scheme that solves the multi-dimensional conservation law

$$\frac{\partial}{\partial t} U + \vec{\nabla} \cdot \vec{F} = 0. \quad (27)$$

A more difficult part in the multi-dimensional IDSA is the consistent solution of Eqs. (7) and (18)-(21). The difficulty arises from the non-local scalar

$$\alpha = \vec{\nabla} \cdot \left(\frac{-1}{3(j + \chi + \phi)} \vec{\nabla} f^t \right) \quad (28)$$

in Eq. (7). The other equations are local and do not depend on the dimensionality of the problem, except that the integration over the angle cosine, $1/2 \int d\mu$, must be replaced by an integration over the entire solid angle of a sphere, $1/(4\pi) \int d\Omega$.

We believe that there are three options when implementing Eq. (28): (i) One may calculate Eq. (28) based on f^t of the previous time step and update f^t locally with Eqs. (18)-(21). Hence, only the local reactions would be implemented implicitly while the diffusion part remains explicit. This approach is only conditionally stable and the time step must be restricted to $\Delta x^2/(2\lambda c)$. The relevance of trapped particles diminishes in the transparent regime around $\lambda \sim \Delta x$. Thus, the time step restriction is of similar order of magnitude as the CFL condition for the particle propagation speed c . As the sound speed in neutron stars is close to the speed of light, the explicit approach may still be a viable option for our application. (ii) In order to obtain an unconditionally stable time step, a global implicit solution of above equations could also be attempted. Because of the source limiting in Eq. (7), the problem is most easily expressed in terms of the unlimited diffusion source Σ as function of $\partial f^t/\partial t$ as outlined in Appendix B in Eqs. (49) and (44). Then, one may search for a globally consistent solution of the field of diffusion sources. This approach has the disadvantage that a spectral problem has to be solved globally, which results in very memory- and cpu-intensive code. The computational effort would become comparable with multi-group flux limited diffusion or even more sophisticated algorithms of radiative transfer. However, the solution could still be restricted to the regimes where the trapped particle component is dominant. (iii) Perhaps the most promising approach is the combination of specific directional sweeps with a locally implicit update of the diffusion source, be it in the form of a Crank-Nicholson scheme with ADI (e.g. Press et al. (1992)) or using Saul'yev's asymmetric updates (Saul'yev 1964; Tavakoli & Davami 2007). This approach leads to an unconditionally stable time step while retaining the efficiency of an explicit scheme. In Appendix B we apply such an approach for our spherically symmetric application.

Independent of the method used, the result of this step determines a partial update of the compositional quantities in U and a spectral diffusion source $\Sigma_l(E)$ for each particle species l at each grid point. This information is stored for the following updates. The stationary-state solution for the streaming particle component is then based on

$$\Delta\psi = \frac{1}{4\pi} \int \left[-(\hat{j} + \hat{\chi}) \hat{f}^s + \hat{\Sigma} \right] d\hat{\Omega}, \quad (29)$$

which is the natural extension of Eq. (10) to the multi-dimensional case. The integration over $d\hat{\Omega}$ is again performed over the solid angle of a sphere. If the relative velocities in the transparent regime are large, the source should be transformed from the comoving frame to the laboratory frame (quantities measured in the laboratory frame carry a hat). Note that Eq. (29) must be solved for each energy group and particle species separately. But all directional information of the streaming particle flux $\vec{\nabla}\psi$ can be retrieved from the corresponding scalar potential $\psi_l(\hat{E})$. Once $\psi_l(\hat{E})$ has been calculated, the equally large field $\Sigma_l(E)$ is no longer needed.

After the hydrodynamic update according to Eq. (27), we have to convert the particle flux, $\vec{\nabla}\psi_l(\hat{E})$, into a streaming particle density. This is now more ambiguous than in Eq. (13). One may still follow the same procedure and first determine the particle scattering spheres. Then, one assumes a flux factor of one half in regions enclosed by the scattering spheres while using an isotropic emission ansatz along the scattering spheres to estimate the flux factor in the domain outside the scattering spheres based on their geometry. For nearly spherical problems such as ours, the much simpler spherically symmetric ansatz described above might even be sufficient to obtain an estimate of the flux factor. Once the spectral streaming particle density $1/(4\pi) \int f_l^s(E) d\Omega$ has been determined by the quotient of $\vec{\nabla}\psi_l(\hat{E})$ and the flux factor, one cycle of updates in a multidimensional application is concluded.

5. CONCLUSION

The isotropic diffusion source approximation (IDSA) has been designed to treat radiative transfer most efficiently in astrophysical applications where particles diffuse out of an opaque domain that is subject to multi-dimensional dynamics. This scenario occurs frequently in new-born gravitationally bound objects, accretion discs, or dynamical atmospheres. We have developed and tested the IDSA in the context of spherically symmetric supernova models. The neutrino transport in core collapse supernovae provides a very challenging application where comprehensive solutions of the Boltzmann transport equation have been studied in great detail (e.g. Mezzacappa (2005) and references therein). Our approximation treats only the most important features of radiative transfer. In a supernova model, these are (i) the thermodynamics of trapped neutrinos (for example the $dE_\nu = -p_\nu dV$ -term), (ii) the correct diffusion limit, (iii) the spectrum of transported neutrinos, and (iv) the angular focussing of the neutrino propagation directions with increasing distance from the neutrinospheres.

We implemented the IDSA in the hydrodynamics code Agile (Liebendörfer et al. 2002) to compare its performance with a more sophisticated transport model. We

compare the postbounce evolution of a $13 M_{\odot}$ star (Nomoto & Hashimoto 1988) in Newtonian gravity with the corresponding model N13 that is based on Boltzmann neutrino transport (Liebendörfer et al. 2005). We find good agreement between the results of the IDSA and the reference model during the early postbounce phase when the neutrino burst is launched and the accretion shock expands to its maximum radius. The IDSA leads to a somewhat larger maximum shock radius and a faster shock retraction thereafter, i.e. a slightly more pessimistic model with respect to the possibility of a delayed supernova explosion. We conclude that the concept of the IDSA accurately captures the feedback of neutrino transport onto the hydrodynamics evolution in spherically symmetric supernova models. The neutrino fluxes and spectra are in nice agreement if small time steps are taken, but unphysical fluctuations in the stationary-state neutrino luminosities develop when the time steps are increased much beyond the neutrino propagation time scale. We will continue to improve the numerical stability of the scheme in future work.

With respect to the choice of physical assumptions and with respect to the quality of the results, the IDSA is most closely related to the well-known flux-limited diffusion (FLD) approximation. Like the latter, the IDSA is guided by the diffusion limit at high opacities and the free streaming limit at low opacities. The FLD approximation is based on diffusive fluxes that are limited by the physical particle speed at the transition to the free streaming regime. This limiting is well-defined in a spherically symmetric setup where the limiting can be applied to the radial velocity direction. In a multi-dimensional simulation, however, FLD fails to determine the correct direction of the net flux outside the diffusive regime. In the free streaming regime there is no physical connection between the local radiation intensity and the flux direction. A related point is the efficiency of the FLD approach. Since the implemented numerical solution strategies are optimised for the diffusive domain, they easily become inefficient in the free streaming regime, which represents often the larger part of the computational domain. These are the two main shortcomings of FLD which we address with the IDSA. The IDSA is based on an overlapping two-component description. The trapped particle component dominates in the diffusive regime while the streaming component dominates in the free streaming regime. In the diffusive regime, the IDSA is equivalent to FLD. In the semi-transparent regime, the IDSA is based on a different interpolation between the diffusive and the free streaming regimes. In the IDSA, the limiter is applied to the sources instead of the fluxes. In the free streaming limit of a multi-dimensional application, the direction of fluxes is well-defined by the non-local position of the sources. The distinction between the trapped and streaming particle components allows us to separately test more efficient solution algo-

rithms for both regimes.

For example, we assumed that the trapped particle component is close to thermal and weak equilibrium while the streaming particle component carries a non-equilibrium spectrum. In the framework of the IDSA we have compared a grey and a spectral (i.e. energy-averaged and energy-dependent) treatment of the evolution of the trapped particle component. We found visible differences of several percent. We believe that the differences are large enough to value the spectral approach, but at the same time they are small enough to be ignored if the efficiency of the algorithm in 3D simulations becomes critical. However, we emphasise that this comparison must not be confused with the comparison of a globally grey scheme and a globally spectral approach. We believe that the *streaming* particle component, which represents the lepton and energy flux in a supernova application, must be treated in a spectral manner. The location of the neutrinospheres is highly energy-dependent. Hence, the geometry of the radiative transfer problem is different for each neutrino energy. An energy-averaged local quantity can only be expected to be accurately represented if one averages over solutions of the energy-dependent transport problem. A grey scheme, that solves an energy-averaged transport problem instead, is unlikely to produce accurate results in the supernova context.

Aside from the field of neutrino-driven supernova models, FLD has been used in fields ranging from planet migration (Paardekooper & Mellema 2006) to cosmology (Bonanno & Romano 1994), including areas such as accretion discs, both around stars (Kley 1989) and more energetic objects where the accretion disc is dominated by radiation (e.g. (Turner et al. 2002; Hujerir & Camenzind 2000)), and star formation (Whitehouse & Bate 2006). The IDSA is potentially applicable to these and other areas of astrophysics where FLD is commonly used. However, neither the IDSA nor the FLDA can replace the development of more reliable transport schemes because, for each application, it has to be ascertained that no important physical ingredients are missed. We hope that the IDSA is well-suited to accompany the application of sophisticated radiative transfer algorithms in order to enable an efficient exploration of input physics, parameter space, or dimensionality in computer models where a comprehensive solution of the Boltzmann transport equation is not affordable.

ACKNOWLEDGEMENTS

This research was funded by the Swiss National Science Foundation under grant No. PP002-106627/1. ML and SCW acknowledge the hospitality of the Institute for Pure and Applied Mathematics at the University of California, Los Angeles, where our collaboration began. We are grateful for prolific discussions with Ue-Li Pen, Tom Abel, Jose Pons, Yudai Suwa and Andrey Yudin.

REFERENCES

- Arnett, W. D., 1966, Canadian Journal of Physics, 44, 2553
- , 1977, ApJ, 218, 815
- Bethe, H. A., 1990, Rev. Mod. Phys., 62, 801
- Bethe, H. A., & Wilson, J. R., 1985, ApJ, 295, 14
- Blondin, J. M., Mezzacappa, A., & DeMarino, C., 2003, ApJ, 584, 971
- Bonanno, A., & Romano, V., 1994, Phys. Rev. D, 49, 6450
- Bowers, R. L., & Wilson, J. R., 1982, apjs, 50, 115
- Bruenn, S. W., 1985, ApJS, 58, 771
- Bruenn, S. W., Mezzacappa, A., Hayes, J. C., Blondin, J. M., Hix, W. R., & Messer, O. E. B., 2006, Journal of Physics Conference Series, 46, 393
- Brunner, S., Valeo, E., & Krommes, J. A., 1999, Physics of Plasmas, 6, 4504

- Burrows, A., Livne, E., Dessart, L., Ott, C. D., & Murphy, J., 2006, *ApJ*, 640, 878
- Burrows, A., Young, T., Pinto, P., Eastman, R., & Thompson, T. A., 2000, *ApJ*, 539, 865
- Castor, J. I., 1972, *ApJ*, 178, 779
- Chapman, S., & Cowling, T. G., 1970, *The mathematical theory of non-uniform gases. an account of the kinetic theory of viscosity, thermal conduction and diffusion in gases* (Cambridge: University Press, 1970, 3rd ed.)
- Chick, K. M., & Cassen, P., 1997, in *Herbig-Haro Flows and the Birth of Stars*, edited by B. Reipurth, & C. Bertout, volume 182 of *IAU Symposium*, pp. 207P–
- Colgate, S. A., & White, R. H., 1966, *ApJ*, 143, 626
- Crouseilles, N., Degond, P., & Lemou, M., 2004, *Journal of Computational Physics*, 199, 776
- Dessart, L., Burrows, A., Livne, E., & Ott, C. D., 2007, *ApJ*, 669, 585
- Epstein, R. I., & Pethick, C. J., 1981, *ApJ*, 243, 1003
- Fryer, C. L., & Warren, M. S., 2004, *ApJ*, 601, 391
- Gnedin, N. Y., & Abel, T., 2001, *New Astronomy*, 6, 437
- Herant, M., Benz, W., Hix, W. R., Fryer, C. L., & Colgate, S. A., 1994, *ApJ*, 435, 339
- Hujeirat, A., & Camenzind, M., 2000, *A&A*, 360, L17
- Kley, W., 1989, *A&A*, 208, 98
- Kotake, K., Sato, K., & Takahashi, K., 2006, *Reports of Progress in Physics*, 69, 971
- Lattimer, J. M., & Swesty, F. D., 1991, *Nucl. Phys. A*, 535, 331
- Levermore, C. D., & Pomraning, G. C., 1981, *ApJ*, 248, 321
- Lieboldörfer, M., Messer, O. E. B., Mezzacappa, A., Bruenn, S. W., Cardall, C. Y., & Thielemann, F.-K., 2004, *ApJS*, 150, 263
- Lieboldörfer, M., Rampp, M., Janka, H.-T., & Mezzacappa, A., 2005, *ApJ*, 620, 840
- Lieboldörfer, M., Rosswog, S., & Thielemann, F.-K., 2002, *ApJS*, 141, 229
- Lieboldörfer, M., 2005, *ApJ*, 633, 1042
- Lieboldörfer, M., Mezzacappa, A., Thielemann, F.-K., Messer, O. E. B., Hix, W. R., & Bruenn, S. W., 2001, *Phys. Rev. D*, 63, 103004
- Lindquist, R. W., 1966, *Annals of Physics*, 37, 487
- Marek, A., & Janka, H., 2007, *ArXiv e-prints*, 708, 0708.3372, 0708.3372
- Mazurek, T. J., 1975, *Astrophys. Space Sci.*, 35, 117
- Messer, O. E. B., Mezzacappa, A., Bruenn, S. W., & Guidry, M. W., 1998, *ApJ*, 507, 353
- Mezzacappa, A., 2005, in *ASP Conf. Ser. 342: 1604-2004: Supernovae as Cosmological Lighthouses*, edited by M. Turatto, S. Benetti, L. Zampieri, & W. Shea, pp. 175–
- Mezzacappa, A., & Bruenn, S. W., 1993, *ApJ*, 405, 669
- Mezzacappa, A., & Messer, O. E. B., 1999, *Journal of Computational and Applied Mathematics*, 109, 281
- Mihalas, D., & Weibel Mihalas, B., 1984, *Foundations of radiation hydrodynamics* (New York: Oxford University Press, 1984)
- Myra, E. S., & Bludman, S. A., 1989, *ApJ*, 340, 384
- Myra, E. S., & Burrows, A., 1990, *ApJ*, 364, 222
- Nomoto, K., & Hashimoto, M., 1988, *Phys. Rep.*, 163, 13
- Ott, C. D., Burrows, A., Dessart, L., & Livne, E., 2008, *ApJ*, 685, 1069
- Ott, C. D., Dimmelmeier, H., Marek, A., Janka, H.-T., Hawke, I., Zink, B., & Schnetter, E., 2007, *Physical Review Letters*, 98, 261101
- Paardekooper, S.-J., & Mellema, G., 2006, *A&A*, 459, L17
- Parker, S. E., & Lee, W. W., 1993, *Physics of Fluids B*, 5, 77
- Press, W. H., Teukolsky, S. A., Vetterling, W. T., & Flannery, B. P., 1992, *Numerical recipes in FORTRAN. The art of scientific computing* (Cambridge: University Press, —c1992, 2nd ed.)
- Rampp, M., & Janka, H.-T., 2002, *A&A*, 396, 361
- Saul'yev, V. K., 1964, *Integration of Equations of Parabolic Type Equation by the Method of Net* (Pergamon Press, New York)
- Scheck, L., Plewa, T., Janka, H.-T., Kifonidis, K., & Müller, E., 2004, *Physical Review Letters*, 92, 011103
- Scheidegger, S., Fischer, T., Whitehouse, S. C., & Liebendörfer, M., 2008, *A&A*, 490, 231
- Sumiyoshi, K., Yamada, S., Suzuki, H., Shen, H., Chiba, S., & Toki, H., 2005, *ApJ*, 629, 922
- Tavakoli, R., & Davami, P., 2007, *Appl. Math. Comput.*, 188, 1184
- Thompson, T. A., Burrows, A., & Pinto, P. A., 2003, *ApJ*, 592, 434
- Turner, N. J., Stone, J. M., & Sano, T., 2002, *ApJ*, 566, 148
- Walder, R., Burrows, A., Ott, C. D., Livne, E., Lichtenstadt, I., & Jarrar, M., 2005, *ApJ*, 626, 317
- Whitehouse, S. C., & Bate, M. R., 2006, *MNRAS*, 367, 32
- Wilson, J. R., 1971, *ApJ*, 163, 209
- Yamada, S., Janka, H.-T., & Suzuki, H., 1999, *A&A*, 344, 533

APPENDIX A: THE DIFFUSION LIMIT REVISITED

Even if the following is old wine in a new hose, we derive the diffusion limit here in brief in order to make a clear distinction between a flux-limited diffusion approximation, which determines the *particle flux* based on the diffusion limit and our scheme, which requires a well-founded approximation for the *collision integral* in the diffusive limit.

The source term on the right hand side of the Boltzmann equation (3) features an isotropic emissivity, j , an isotropic absorptivity, χ , and an isoenergetic scattering kernel, R . For the derivation of the diffusion limit, the angular dependence of the scattering kernel is usually expanded in a Legendre series (see e.g. Bruenn (1985); Mezzacappa & Bruenn (1993)),

$$\frac{E^2}{c(hc)^3} R(E, \mu, \mu') = \frac{1}{4\pi} \sum_{\ell} (2\ell + 1) \phi_{\ell}(E) \int_0^{2\pi} P_{\ell}(\cos \theta) d\varphi, \quad (30)$$

where $\cos \theta = \mu\mu' + \cos \varphi [(1 - \mu^2)(1 - \mu'^2)]^{1/2}$ specifies the angle between the incoming and the scattered particle propagation directions. In Eq. (30) we define $\phi_{\ell}(E)$ such that it enters Eq. (3) without additional factors. If we denote the operator on the left hand side of Eq. (3) by $D(f)$ and truncate the Legendre expansion after the second term, we reach a very concise representation of the Boltzmann equation,

$$D(f) = j - (j + \chi + \phi_0) f + \phi_0 \frac{1}{2} \int_{-1}^{+1} f d\mu + 3\mu\phi_1 \frac{1}{2} \int_{-1}^{+1} f \mu d\mu. \quad (31)$$

From the zeroth and first angular moments of Eq. (31) we extract an expression for the zeroth and first moments of the distribution function, respectively,

$$\begin{aligned} \frac{1}{2} \int f d\mu &= \frac{1}{j + \chi} \left(j - \frac{1}{2} \int D(f) d\mu \right), \\ \frac{1}{2} \int f \mu d\mu &= \frac{-1}{j + \chi + \phi_0 - \phi_1} \frac{1}{2} \int D(f) \mu d\mu. \end{aligned} \quad (32)$$

If we substitute these terms back into Eq. (31), we can express the distribution function f in the following way,

$$f = \frac{1}{j + \chi + \phi_0} \left\{ j - D(f) + \frac{\phi_0}{j + \chi} \left[j - \frac{1}{2} \int D(f) d\mu \right] - \frac{\mu\phi_1}{j + \chi + \phi_0 - \phi_1} \frac{1}{2} \int D(f) \mu d\mu \right\}. \quad (33)$$

Now, we perform a Chapman-Enskog expansion (Chapman & Cowling 1970). To this purpose we introduce a small expansion parameter, ε , and replace the large source functions j , χ and $\phi_{0,1}$ in Eq. (33) by \bar{j}/ε , $\bar{\chi}/\varepsilon$ and $\bar{\phi}_{0,1}/\varepsilon$, respectively. From the zeroth order terms in ε we then obtain as expected the isotropic equilibrium distribution function $f_0 = j/(j + \chi)$. However, we can also determine the first order corrections to the equilibrium distribution function:

$$\varepsilon f_1 = \frac{-1}{j + \chi + \phi_0} \left[D(f_0) + \frac{\phi_0}{j + \chi} \frac{1}{2} \int D(f_0) d\mu + \frac{\mu\phi_1}{j + \chi + \phi_0 - \phi_1} \frac{1}{2} \int D(f_0) \mu d\mu \right]. \quad (34)$$

After these preparations, we obtain the leading order particle number exchange rate with matter, s , by substituting the approximate distribution function $f \simeq f_0 + \varepsilon f_1$ into Eq. (31) and integrating the left hand side over particle propagation angles:

$$s = \frac{1}{2} \int D(f_0 + \varepsilon f_1) d\mu. \quad (35)$$

This integral can be simplified if one decomposes the operator $D(f)$ into an operator $D^+(f)$ containing terms that are symmetric in μ and an operator $D^-(f)$ containing terms that are antisymmetric in μ . Hence, $D(f) = D^+(f) + D^-(f)$, with

$$\begin{aligned} D^+(f) &= \frac{df}{cdt} + \left(\frac{\partial \ln \rho}{c\partial t} + \frac{3v}{cr} \right) \mu (1 - \mu^2) \frac{\partial f}{\partial \mu} + \left[\mu^2 \left(\frac{\partial \ln \rho}{c\partial t} + \frac{3v}{cr} \right) - \frac{v}{cr} \right] E \frac{\partial f}{\partial E} \\ D^-(f) &= \mu \frac{\partial f}{\partial r} + \frac{1}{r} (1 - \mu^2) \frac{\partial f}{\partial \mu}. \end{aligned} \quad (36)$$

Only the symmetric terms $D^+(f_0)$, $D^+[D^+(f_0)]$ and $D^-[D^-(f_0)]$ survive the angular integration in Eq. (35). Furthermore, we may neglect the $D^+[D^+(f)]$ terms because they are of higher order in the expansion than the leading $1/2 \int D^+(f_0) d\mu$ term. The $D^-[D^-(f_0)]$ terms, however, are of leading order because there is no lower order contribution involving D^- . The intermediate result

$$\frac{1}{2} \int D(\varepsilon f_1) d\mu = \frac{1}{2} \int D^- \left(\frac{-1}{j + \chi + \phi_0} \left[D^-(f_0) + \frac{\mu\phi_1}{j + \chi + \phi_0 - \phi_1} \frac{1}{2} \int D^-(f_0) \mu d\mu \right] \right) d\mu \quad (37)$$

can be further simplified if one explicitly calculates the integral in the last term using $D^-(f_0) = \mu \partial f_0 / \partial r$. This leaves us with the following leading order source terms in the diffusion limit,

$$s = \frac{1}{2} \int D^+(f_0) d\mu - \frac{1}{2} \int D^- \left(\frac{1}{j + \chi + \phi_0 - \phi_1} D^-(f_0) \right) d\mu. \quad (38)$$

The original operators in Eq. (36) may now be readily substituted. Several $\partial/\partial\mu$ -terms drop out due to the isotropy of $f_0 = j/(j + \chi)$ and the remaining angular integrations can easily be performed. With this, we obtain the following simple expression for the collision integral in the diffusion limit,

$$s = \frac{df_0}{cdt} + \frac{1}{3} \frac{\partial \ln \rho}{c\partial t} E \frac{\partial f_0}{\partial E} - \frac{1}{r^2} \frac{\partial}{\partial r} \left(\frac{r^2}{3(j + \chi + \phi)} \frac{\partial f_0}{\partial r} \right), \quad (39)$$

where, in order to shorten the notation, we define $\phi = \phi_0 - \phi_1$. Note that a flux-limited diffusion scheme applies Eq. (39) as evolution equation for an unknown $f(t, r, E)$ (instead of f_0) together with a source function $s(f)$. Our scheme uses Eq. (39) as leading order approximation to the source s for a given equilibrium distribution function f_0 , exactly as derived. The first term in Eq. (39) describes sources that arise from adjustments to a time-dependent equilibrium, the second term accounts for changes in the average particle energy when the fluid is compressed or expanded and the third term describes the divergence of the diffusive flux in the rest frame of the fluid according to the transport mean free path $\lambda_t = (j + \chi + \phi)^{-1}$.

APPENDIX B: IMPLEMENTATION AND FINITE DIFFERENCING

In this appendix we discuss the finite differencing of our implementation of the IDSA. Our scheme solves Eq. (18) for the trapped particles, Eq. (10) for the streaming particles, and Eq. (14) for the hydrodynamics in an operator splitting manner. The spherically symmetric computational domain is represented by an array of concentric fluid shells labelled by the index $i = 1 \dots i_{max}$. Unprimed indices are used for zone centre values and primed indices for the upper zone edge values. Energy-dependent quantities are calculated for a set of discrete particle energies E_k , where $k = 1 \dots k_{max}$. This representation exists for several time instances, which we label by an upper index $n = 1 \dots n_{max}$. For example, $\lambda_{i,k}^n$ refers to the mean free path $\lambda(r_{i+1/2}, E_k, t^n)$ at the zone edge between r_i and r_{i+1} , at energy E_k and at time t^n .

A time steps begins with the construction of the particle flux at time t^{n+1} from the particle sources, $\Sigma - (j + \chi) \frac{1}{2} \int f^s d\mu$, which have been calculated and stored during the previous time step t^n . The particle flux is given by the gradient of the potential ψ as described in Eq. (10). In spherical symmetry, this Poisson equation is easily solved by the integration of the sources over the volume,

$$\left(\frac{\partial\psi}{\partial r}\right)_{i',k}^{n+1} = \frac{1}{r_{i'}^2} \sum_{j=1}^{j=i'} \left[\Sigma_{j,k}^n - \tilde{\chi}_{j,k}^n \frac{1}{2} \int f_{j,k}^{s,n} d\mu \right] r_j^2 (r_{j'} - r_{j'-1}), \quad (40)$$

where we used a tilde to denote stimulated absorption $\tilde{\chi} = j + \chi$. At present we neglect the Lorentz transformation of the sources from the comoving frame to the laboratory frame.

Next, we retrieve the current conditions from the solution vector $U_i^n = U(r_i, t^n)$ and calculate the energy-dependent transport mean free path $\lambda_{i,k}^n$ and the optical depth $\tau_{i,k}^n = \int_{r_i}^{\infty} (1/\lambda(r)_k^n) dr$. In spherical symmetry, the energy-dependent radius $R_{\nu,k}^n$ of the neutrinosphere is found at the point where $\tau(R_{\nu,k}^n) = 2/3$. The neutrinosphere is then used to derive the streaming particle density from the streaming particle flux according to Eq. (13). Again, we neglect the Lorentz transformation between the laboratory and comoving frames and approximate the streaming particle density by

$$\frac{1}{2} \int f_{i,k}^{s,n+1} d\mu = \frac{2}{1 + \sqrt{1 - [R_{\nu,k}^n / \max(r, R_{\nu,k}^n)]^2}} \left(\frac{r_{i'-1}}{r_i}\right)^2 \max \left[\left(\frac{\partial\psi}{\partial r}\right)_{i'-1,k}^{n+1}, 0 \right]. \quad (41)$$

The factor $(r_{i'-1}/r_i)^2$ converts the flux from the inner zone edge $i' - 1$, where it has been calculated in Eq. (40), to the zone centre r_i , where it is used in the calculation of the diffusion source. Two measures significantly increase the stability of the scheme. On the one hand it is important to exclude the contribution of zone i to the streaming particle flux. On the other hand, the maximum function with the square brackets eliminates fluxes that stream against the density gradient.

The trapped particle distribution functions are separated into a thermal component, and a spectral perturbation,

$$f_{i,k}^{t,n} = f_k^{\text{th}}(Y_i^{t,n}, Z_i^{t,n}) + \delta f_{i,k}^{t,n}. \quad (42)$$

The thermal part is represented by a Fermi function, f_k^{th} , where the particle temperature and particle degeneracy are chosen such that Eq. (16) is fulfilled for the current values of the quantities $Y_i^{t,n}$ and $Z_i^{t,n}$ in the solution vector U_i^n . If the analytical approximations given in (Epstein & Pethick 1981) are used, a consistent set of the particle temperature and degeneracy parameters can be obtained from the solution of a one-dimensional Newton-Raphson scheme. For the standard version of the IDSA we neglect the perturbations by setting $\delta f_{i,k}^{t,n} \equiv 0$. In order to test this approximation in Sect. 3, we implemented a second version of the IDSA, where the deviation of the trapped particle spectrum from the thermal spectrum is evolved in time as described in Eq. (55).

The next step is the search for a consistent solution of Eqs. (18), (20) and (21). In most of the following monochromatic equations, all quantities carry the same energy index k . To further reduce the amount of indices we will write the energy index only if quantities at different energies are involved in one equation. We discretise the fast reaction rates on the right hand side of Eq. (18) in a time-implicit way,

$$\frac{f_i^{t,n+1} - f_i^{t,n}}{c\Delta t} = j_i^{n+1} - \tilde{\chi}_i^{n+1} f_i^{t,n+1} - \Sigma_i^{n+1}, \quad (43)$$

and eliminate the dependence on $f_i^{t,n+1}$ on the right hand side by rewriting Eq. (43) in the form

$$\frac{f_i^{t,n+1} - f_i^{t,n}}{c\Delta t} = \frac{j_i^{n+1} - \tilde{\chi}_i^{n+1} f_i^{t,n} - \Sigma_i^{n+1}}{1 + \tilde{\chi}_i^{n+1} c\Delta t}. \quad (44)$$

The diffusion source Σ , which is defined in Eq. (7), depends on α . We will work with the following definition of α :

$$\xi_i = \frac{1}{3r_i^2 (r_{i'} - r_{i'-1})} \frac{r_{i'}^2 \lambda_{i'}}{r_{i+1} - r_i} \quad (45)$$

$$\zeta_i = \frac{1}{3r_i^2 (r_{i'} - r_{i'-1})} \frac{r_{i'-1}^2 \lambda_{i'-1}}{r_i - r_{i-1}} \quad (46)$$

$$\eta_i = \xi_i + \zeta_i \quad (47)$$

$$\alpha_i = -\xi_i f_{i+1}^t + \eta_i f_i^t - \zeta_i f_{i-1}^t. \quad (48)$$

In the search for a consistent diffusion source we first assume that $\tilde{\Sigma} = \alpha + \tilde{\chi} \frac{1}{2} \int f^s d\mu$ is not limited. Then we apply the limiters in Eq. (7) to the result. It is known that the numerical evolution of the diffusion equation is not

unconditionally stable unless the term α is finite differenced in an at least partially implicit manner (e.g. Press et al. (1992)). Hence, we would like to discretise the diffusion source as

$$\tilde{\Sigma}_i^{n+1} = -\xi_i^n (f_{i+1}^{t,n+1} - f_{i+1}^{t,n}) + \eta_i^n (f_i^{t,n+1} - f_i^{t,n}) - \zeta_i^n (f_{i-1}^{t,n+1} - f_{i-1}^{t,n}) + \alpha_i^n + \tilde{\chi}_i^{n+1} \frac{1}{2} \int f_i^{s,n+1} d\mu. \quad (49)$$

The dependence of this equation on the unknown distribution functions $f_i^{t,n+1}$ can be removed if we substitute Eq. (44) in the first three terms. The result is a non-local equation involving $\tilde{\Sigma}_{i+1}^{n+1}$, $\tilde{\Sigma}_i^{n+1}$ and $\tilde{\Sigma}_{i-1}^{n+1}$, which could globally be solved for $\tilde{\Sigma}_i^{n+1}$. However, since our target application is based on a three-dimensional parallelised hydrodynamics code, for the moment we try to avoid a global solution of Eqs. (49) and (44). At least in our spherically symmetric example, the diffusive fluxes propagate almost exclusively outward. Hence we finite difference the outward propagating flux implicitly and the inward propagating flux explicitly, which leads to

$$\tilde{\Sigma}_i^{n+1} = \zeta_i^n (f_i^{t,n+1} - f_i^{t,n}) - \zeta_i^n (f_{i-1}^{t,n+1} - f_{i-1}^{t,n}) + \alpha_i^n + \tilde{\chi}_i^{n+1} \frac{1}{2} \int f_i^{s,n+1} d\mu. \quad (50)$$

If one applies Eq. (50) from the inside out, $f_{i-1}^{t,n+1}$ is known from the update of the previous zone. After substitution of Eq. (44) in the first term, Eq. (50) can be solved for $\tilde{\Sigma}_i^{n+1}$ so that the limiter from Eq. (7) can be applied,

$$\begin{aligned} \Sigma_i^{n+1} &= \min \left\{ \max \left[\tilde{\Sigma}_i^{n+1}, 0 \right], j_i^{n+1} \right\} \\ \tilde{\Sigma}_i^{n+1} &= \frac{1}{1 + (\zeta_i^n + \tilde{\chi}_i^{n+1}) c\Delta t} \left\{ \zeta_i^n c\Delta t (j_i^{n+1} - \tilde{\chi}_i^{n+1} f_i^{t,n}) + (1 + \tilde{\chi}_i^{n+1} c\Delta t) \right. \\ &\quad \times \left. \left[-\xi_i^n f_{i+1}^{t,n} + \eta_i^n f_i^{t,n} - \zeta_i^n f_{i-1}^{t,n+1} + \tilde{\chi}_i^{n+1} \frac{1}{2} \int f_i^{s,n+1} d\mu \right] \right\}. \end{aligned} \quad (51)$$

This diffusion source Σ_i^{n+1} can now be used in Eq. (44) to determine the discrete time derivative of the trapped particle distribution function, $(f_i^{t,n+1} - f_i^{t,n}) / (c\Delta t)$. Furthermore, this derivative specifies the net interaction rate between matter and trapped particles, which can be calculated according to Eq. (19),

$$s_i^{n+1} = \frac{f_i^{t,n+1} - f_i^{t,n}}{c\Delta t} + \Sigma_i^{n+1} - \tilde{\chi}_i^{n+1} \frac{1}{2} \int f_i^{s,n+1} d\mu. \quad (52)$$

In the application of Eq. (51) to the supernova model in Sect. 3 we observed a slightly too rapid deleptonisation few milliseconds after the bounce of the stellar core. As the dynamical time scale of the bounce is comparable to the neutrino propagation time scale in this short transition phase, the stationary-state assumption of our approximation may not hold. This effect disappeared when we additionally limited Σ in Eq. (51) by $f_i^{t,n+1}/\Delta r$, where $\Delta r \sim 15$ km is an empirically determined constant parameter.

In the case of neutrino transport with electron neutrinos and electron antineutrinos Eq. (52) leads to the following updates of the electron fraction and the internal specific energy in Eqs. (20) and (21):

$$\frac{Y_{e,i}^{n+1} - Y_{e,i}^n}{c\Delta t} + \frac{m_b}{\rho_i^n} \frac{4\pi}{(hc)^3} \sum_k \left(s_{\nu_e,i,k}^{n+1} - s_{\bar{\nu}_e,i,k}^{n+1} \right) E_k^2 dE_k = 0 \quad (53)$$

$$\frac{e_i^{n+1} - e_i^n}{c\Delta t} + \frac{m_b}{\rho_i^n} \frac{4\pi}{(hc)^3} \sum_k \left(s_{\nu_e,i,k}^{n+1} + s_{\bar{\nu}_e,i,k}^{n+1} \right) E_k^3 dE_k = 0. \quad (54)$$

However, the neutrino-matter interactions $j_i^{n+1} = j(\rho_i^n, Y_{e,i}^{n+1}, e_i^{n+1})$ and $\chi(\rho_i^n, Y_{e,i}^{n+1}, e_i^{n+1})$, which enter the right hand sides of Eqs. (53) and (54) via Eq. (44), depend on the updated values for the electron fraction and specific internal energy. Hence we solve this nonlinear algebraic system of equations numerically by two-dimensional Newton-Raphson iterations to determine a consistent $\{Y_{e,i}^{n+1}, e_i^{n+1}\}$ -pair¹. This consistency is important to accurately represent reactive equilibria at high opacities. Following an approach of Mezzacappa & Messer (1999), we first evaluate Eq. (52) on four corners of a rectangle, centred around the initial values $\{Y_{e,i}^n, e_i^n\}$ in the space spanned by electron fraction and specific energy. Then, we use interpolations in this rectangle to efficiently obtain the reaction rates and their derivatives with respect to Y_e and e during the iterations required to find a consistent solution of Eqs. (53) and (54). Once the iterations have converged, we update ρY_e and ρe in the hydrodynamics state vector $U^{n'}$, where n' indicates an intermediate incomplete update.

Finally, the components ρY^t and $(\rho Z^t)^{3/4}$ in U^n are updated based on Eqs. (22), (23) and (44). In the standard version of the IDSA, the spectral information of the trapped particle component is discarded at this point. For the

¹ In fact, for compatibility reasons with the hydrodynamics code and the equation of state, our implementation of the Newton-Raphson scheme works with the logarithmic entropy instead of the specific energy.

alternative version, the spectral information is stored in an energy-dependent vector $\delta f_{i,k}^{t,n+1}$ that will be used in the next time step according to Eq. (42). The latter is obtained from

$$\begin{aligned}
 \delta f_k^* &= f_{i,k}^{t,n+1} - f_k^{\text{th}} \left(Y_i^{t,n+1}, Z_i^{t,n+1} \right) \\
 \delta f_{i,k}^{t,n+1} &= \delta f_k^* + \frac{a_0 b_2 - a_1 b_1 - (a_0 b_1 - a_1 b_0) E_k}{(b_1^2 - b_0 b_2)} f_k^{\text{th}} \left(Y_i^{t,n+1}, Z_i^{t,n+1} \right) \\
 a_m &= \sum_k \delta f_k^* E_k^{2+m} dE_k \\
 b_m &= \sum_k f_k^{\text{th}} \left(Y_i^{t,n+1}, Z_i^{t,n+1} \right) E_k^{2+m} dE_k.
 \end{aligned} \tag{55}$$

The first line in Eq. (55) calculates the deviation between the updated trapped particle distribution function and the thermal spectrum. Due to numerical inaccuracies, spurious errors can accumulate in δf_k^* over many time steps and start to contribute to the trapped particle abundance Y_i^t and the mean specific energy Z_i^t which should be determined by the thermal part alone. Adding the correction term on the second line of Eq. (55) guarantees that $\sum \delta f_{i,k}^{t,n+1} E_k^2 dE_k = 0$ and $\sum \delta f_{i,k}^{t,n+1} E_k^3 dE_k = 0$ to machine precision. The correction term depends on energy moments of δf_k^* and the thermal distribution function.

The cycle of updates is concluded by evolving the partially updated hydrodynamics state $U^{n'}$ to U^{n+1} according to Eq. (14) (and including gravity) by any standard hydrodynamics scheme. For this demonstration of the method we use the spherically symmetric hydrodynamics code Agile (Liebendörfer et al. 2002) with a second order accurate TVD advection scheme.